Published in Boreas 46 (2017) 541–561

Influence of the Laurentide Ice Sheet and relative sea-level changes on sediment dynamics in the Estuary and Gulf of St. Lawrence since the last deglaciation

Marie Casse, Jean-Carlos Montero-Serrano, Guillaume St-Onge

Physical properties, grain size, bulk mineralogy, elemental geochemistry, and magnetic parameters of three sediment piston cores recovered in the Laurentian Channel from its head to its mouth were investigated to reconstruct changes in detrital sediment provenance and transport related to climate variability since the last deglaciation. The comparison of the detrital proxies indicates the succession of two sedimentary regimes in the Estuary and Gulf of St. Lawrence (EGSL) during the Holocene, which are associated with the melting history of the Laurentide Ice Sheet (LIS) and relative sea level changes. During the early Holocene (10–8.5 ka cal BP), high sedimentation rates together with mineralogical, geochemical, and magnetic signatures indicate that sedimentation in the EGSL was mainly controlled by meltwater discharges from the local retreat of the southeastern margin of the LIS on the Canadian Shield. At this time, sediment-laden meltwater plumes caused the accumulation of fine-grained sediments in the ice-distal zones. Since the mid-Holocene, postglacial movements of the continental crust, related to the withdrawal of the LIS (~6 ka cal BP), have triggered significant variations in relative sea level (RSL) in the EGSL. The significant correlation between the RSL curves and the mineralogical, geochemical, magnetic, and grain-size data suggest that the RSL was the dominant force acting on the sedimentary dynamics of the EGSL during the mid-to-late Holocene. Beyond 6 ka cal BP, characteristic mineralogical, geochemical, magnetic signatures and diffuse spectral reflectance data suggest that the Canadian Maritime Provinces and western Newfoundland coast are the primary sources for detrital sediments in the Gulf of St. Lawrence, with the Canadian Shield acting as a secondary source. Conversely, in the lower St. Lawrence Estuary, detrital sediments are mainly supplied by the Canadian

Shield province. Finally, our results suggest that the modern sedimentation regime in the EGSL was established during the mid-Holocene.

Keywords: Estuary and Gulf of St. Lawrence; Holocene; Laurentide Ice Sheet; relative sea level; bulk mineralogy; elemental geochemistry; magnetic properties.

Marie Casse [Marie.Casse@uqar.ca, marie64casse@gmail.com], Jean-Carlos Montero-Serrano [jeancarlos_monteroserrano@uqar.ca], Guillaume St-Onge [Guillaume_St-Onge@uqar.ca], Institut des sciences de la mer de Rimouski, Canada Research Chair in Marine Geology, Université du Québec à Rimouski & GEOTOP, 310 allée des Ursulines, Rimouski, Québec, G5L 3A1, Canada.

1. Introduction

During the early Holocene (11.5–5 ka cal BP), high boreal summer insolation drove rapid retreat of the Laurentide Ice Sheet (LIS), resulting in progressive changes in the North American climate (e.g., COHMAP Members, 1988; Webb et al., 1998; Carlson et al., 2007; Montero-Serrano et al., 2009, 2010, 2011). During this early stage, the hydrological and sedimentary characteristics of the Estuary and Gulf of St. Lawrence (EGSL) in eastern Canada were heavily disturbed by meltwater discharges from the LIS southeastern margin and subsequent relative sea-level (RSL) variations (e.g., Dyke and Prest, 1987; Shaw et al., 2002, 2006; St-Onge et al., 2011; Levac et al., 2015). Indeed, modifications in deglacial meltwater inputs via the St. Lawrence drainage system as the southern LIS margin retreated caused abrupt changes in sedimentation rates in the EGSL, with rates higher than ~30 m/ka during the initial deglaciation and lower rates (~40–67 cm/ka) during the early-to-late Holocene (e.g., St-Onge et al., 2003; Barletta et al., 2010).

In addition to impacting sedimentation rates in the EGSL, the LIS retreat also caused significant variations in relative sea level due to glacio-isostatic rebound (Shaw et al., 2002, 2006; Rémillard et al., in press). In the EGSL, the LIS deglacial retreat exposed large areas of isostatically depressed land that were rapidly submerged (~ +130 m above present levels) by the transgression of the Goldthwait Sea (Dionne, 1977). After ice retreat, postglacial rebound in this area caused sea level to quickly drop below present levels (~ -20 m) before they rose once more through the Holocene (e.g., Shaw et al., 2002). The transition from open (glacial) marine to estuarine sedimentation in the EGSL is therefore controlled by glacio-isostatic relative sea-level variations. However, the timing and magnitude of this postglacial isostatic rebound in the EGSL, and therefore of RSL, vary spatially depending on both the ice thickness and the location of a particular area relative to the ice margin (Licciardi et al., 1999; Dyke and Peltier, 2000; Dionne, 2001; Shaw et al., 2002; 2006; Rémillard et al., 2016). The postglacial sedimentation history in the EGSL is therefore likely a product of changes in the timing and magnitude of sediment flux, glacio-isostatic adjustment, and relative sea-level variations caused by the melting and reatreat of the LIS.

The high sedimentation rates (~40–67 cm/ka; Barletta et al., 2010), together with the relatively fine-grained postglacial sediments recorded in the Laurentian Channel, offer a unique opportunity for reconstructing sediment dynamics and past climate conditions at the centennial to millennial timescales. However, in spite of these exceptional sedimentary characteristics, the nature, origin, and transport of detrital sediments in the EGSL as well as its variability over time have been poorly documented (e.g., D'Anglejan, 1969; D'Anglejan and Smith, 1973; Pinet et al., 2011). Moreover, mineralogical, geochemical, and magnetic signatures of the terrigenous components transported by rivers of the north and south coasts towards the EGSL are specific to the drainage areas where the two main geological provinces (Greenville and Appalachian) contain different bulk mineral assemblages and geochemical signatures (e.g., Loring and Nota, 1973; Jaegle, 2015). These proxies may therefore help to highlight the evolution of sedimentary inputs in the EGSL since the last deglaciation.

Using a multi-proxy approach (including physical properties, magnetic parameters, grain size, bulk mineralogy, and elemental geochemistry) on three piston cores recovered along an east–west transect in the Laurentian Channel (from its head to its mouth), we aim to: (1) reconstruct changes in sediment provenance and transport related to climatic and oceanographic variability and (2) provide new insights on potential relations between sea-level variations and sediment dynamics in the EGSL since the last deglaciation.

2. Physiographic and geological setting of the Estuary and Gulf of St. Lawrence

The EGSL is a transitional environment between the St. Lawrence River and the northwest Atlantic Ocean. Circulation in the EGSL is therefore estuarine, with a less salted surface layer flowing seawards and saltier intermediate and deep layers flowing landwards (Koutitonsky and Bugden, 1991).

Large seasonal contrasts in surface waters range from freezing conditions in winter (allowing the formation of sea ice) to temperate conditions in summer due to a very strong seasonal cycle in the overlying air temperature (e.g., Saucier, 2003; de Vernal et al., 2011).

The annual mean circulation in the EGSL is principally characterized by coastal currents that dominantly flow in an E–W direction (such as, Gaspé Current), the Anticosti Gyre, and by the inflowing West Newfoundland Current that flows northward along the west coast of Newfoundland (**Figure 1a**). These currents are characterized by a mean speed of order ~1 cm/s (Tang and Bennett, 1981). In the EGSL, one of the most striking features of near surface circulation is the Gaspé Current, which is a buoyancy-driven coastal jet originating in the St. Lawrence Estuary (near Rimouski) and flowing seaward along the coast of the Gaspé Peninsula (Sheng, 2001). This current disperses the South Shore St. Lawrence runoff into the northwestern and the southern Gulf (e.g., Loring and Nota, 1973). In addition, according to circulation models from the EGSL (Galbraith et al., 2016), currents are the strongest in the surface mixed layer, generally 0-20 m (**Figure 1a**), except during the winter months when the 20-100 m and the 100 m to bottom averages are almost as high (Galbraith et al., 2016). Currents are also the strongest along the slopes of the deep channels such as the Laurentian Channel (Galbraith et al., 2016).

The EGSL bathymetry is profoundly marked by a submarine U-shaped valley resulting from Quaternary glacial erosion and deposition — the Laurentian Channel (King and MacLean, 1970; Loring and Nota, 1973; Piper et al., 1990). This dominant topographic feature (250–500 m deep) extends from the eastern Canadian continental shelf to the mouth of the Saguenay Fjord near Tadoussac and contains a very thick (>450 m) Quaternary sedimentary sequence (Duchesne et al., 2010; St-Onge et al., 2008). This thick infill is mainly attributable to high sedimentation rates (~100–400 cm/ka; Barletta et al., 2010) driven by the rapid hinterland retreat of the LIS during the last deglaciation and its subsequent meltwater discharges transported into the EGSL via the St. Lawrence River system (e.g., St-Onge et al., 2003, 2008; Mattheus et al., 2007). Likewise, high-resolution seismic reflection data in conjunction with piston coring indicate that tills, glaciomarine sediments, and postglacial muds characterize the regional stratigraphy of the EGSL for the late Pleistocene to Holocene (e.g., Loring and Nota, 1973; Josenhans and Lehman, 1999; Duchesne et al., 2010; St-Onge et al., 2011). Moreover, surface sediments in the EGSL are characterized by fine-grained sediments (notably, fine silts) in the deep central parts of the Laurentian Channel and by coarser-grained sediments (gravels, sands and, to a lesser proportion, fine silts) in the slopes and adjacent shelves (Loring and Nota, 1973; St-Onge et al., 2003; Pinet et al., 2011; Jaegle, 2015).

Total suspended matter in the EGSL is about 60–90% detrital (e.g., D'Anglejan and Smith, 1973). Detrital sedimentation in this area is influenced by seasonal changes in rain and snow precipitation on the continent, freshwater discharges, atmospheric circulation, tidal current, wave energy, and by the formation of sea ice (e.g., D'Anglejan and Smith, 1973; Saucier, 2003; Hargrave et al., 2007; Scully and Friedrich, 2007; Anne de Vernal et al., 2011). In fact, nearshore sediment dynamics of the EGSL are dominated by sea ice (e.g., Dionne, 1993; Neumeier, 2011), with its capacity to transport sediments from clay to boulders, erode tidal marshes and tidal flats, and, thus, participate in the regional erosion budget (Drapeau et al., 1992).

On the other hand, sedimentary inputs in the EGSL derive mainly from the Grenvillian metamorphic rocks of the Canadian Shield on the North Shore as well as from the early Paleozoic sedimentary rocks of the Appalachian domain on the South Shore, Canadian Maritime Provinces, and western Newfoundland coast (Loring and Nota, 1973; Jaegle, 2015). These two geological provinces have drastically different mineralogical, geochemical, and magnetic signatures (**Figure 1b**): (1) Grenvillian metamorphic rocks are characterized by high amphibole, potassium (K) feldspar, plagioclase feldspar, and magnetite contents as well as high magnetic susceptibility, whereas (2) Paleozoic sedimentary rocks of the Appalachian domain are characterized by high quartz, phyllosilicates (mainly biotite and muscovite) and hematite contents, and low magnetic susceptibility (Loring and Nota, 1973;

Jaegle, 2015). In addition, the Paleozoic sedimentary rocks (including limestone, dolostone, and calcareous shale) cropping out on Anticosti Island and the western Newfoundland coast may also contribute local detrital sediments to the Gulf of St. Lawrence (e.g., Loring and Nota, 1973; Ebbestad and Tapanila, 2005). Overall, an important conclusion to draw from these studies is that mineralogical, geochemical, and magnetic variations recorded in the Laurentian Channel sediments may be attributed to changes in the relative contributions of sources of sediment transported by the rivers, sea ice, and tidal currents from the north and south coasts.

3. Material and methods

3.1. Samples

Three sediment cores from the lower St. Lawrence Estuary (COR0602-36PC) and Gulf of St. Lawrence (COR0503-CL04-36 and COR0503-CL04-37) were collected on board the research vessel (R/V) Coriolis II during two different cruises in June 2005 (COR0503) and 2006 (COR0602). These sediment cores were recovered along the axis of the Laurentian Channel, from its head to its mouth (**Table 1; Figure 1b**) using a piston corer, allowing the sampling of cores up to 7.90 m in diameter. All coring sites were targeted using high-resolution seismic profiles that indicated high sediment accumulation not influenced by mass wasting events (Barletta et al., 2010).

Samples for bulk mineralogical analysis were evenly sampled at 5-cm intervals (total of 456 samples). Complementarily, major and minor element concentrations were determined at 15-cm intervals, whereas sediment grain-size analyses were performed at 10-cm intervals. Before the bulk mineralogical and geochemical analysis and in order to isolate the detrital fraction from these sediment samples, organic matter and biogenic carbonate were removed with 10 mL of peroxide (30%) and 10 mL of hydrochloric acid (0.5 M), respectively. Biogenic silica was not removed as it appeared to be negligible (likely less than 1%, as suggested by its no detection in the bulk sediment XRD diffractograms). Next, sediment samples were rinsed five times with distilled water and ground with a McCrone micronizing mill with agate grinding elements to obtain a consistent grain size of <10 µm using 5 mL of ethanol and grinding times of 5–10 min to obtain a homogenous powder. The slurry was oven dried overnight at about 60°C and then slightly homogenized with an agate mortar to prevent the possible agglomeration of finer particles during drying. Aliquots of these homogenized sediment samples were used for bulk mineralogical and geochemical analysis.

3.2. Chronostratigraphic framework

The chronostratigraphic framework of all sediment cores used in this study was published previously and derived from 17 AMS-^{14}C ages obtained on marine mollusc shell fragments (Barletta et al., 2010). Further support of the age model of core COR0602-36PC comes from the lower part (562 cm) by the comparison of magnetic susceptibility profiles with nearby core MD99-2221 (St-Onge et al., 2003) (Figure S1 in the **supplementary material**). Characteristic peaks in both magnetic susceptibility curves have been identified in order to transfer the age model of core MD99-2221 on the core COR0602-36PC below 562 cm where no radiocarbon ages are available for core COR0602-36PC. The R software package BACON (Blaauw and Christen, 2011) was used to produce the "best fit" linearly interpolated age models. BACON uses a Bayesian approach to estimate the best fit or weighted mean age for each depth with a 95% confidence interval. Overall, the chronostratigraphic framework of all these sediment cores suggests high sedimentation rates in the last 10 ka cal BP (300 to 40 cm/ka; **Figure 2**).

3.3. Analytical procedure

3.3.1. *Physical properties: Multisensor Core Logger analyses*

The physical properties were measured using a GEOTEK Multi Sensor Core Logger (MSCL) at the Institut des sciences de la mer de Rimouski (ISMER). Diffuse spectral reflectance data were acquired at 5-cm resolution immediately after splitting the core, using an X-Rite DTP22 hand-held spectrophotometer and are reported in the L*, a*, b* colour space of the International Commission on Illumination (CIE). L* is a black to white scale, a* is a green to red scale, and b* is a blue to yellow scale (e.g., St-Onge et al., 2007; Debret et al., 2011). Note that a* was only used in this study because this can be a useful parameter to detect changes in the concentration of high-coercivity red minerals such as hematite (St-Onge and Lajeunesse, 2007).

3.3.3. *Grain size distribution and end-member modelling analysis*

Sediment grain-size analyses were performed on bulk sediment samples using a Beckman Coulter LS13320 laser diffraction grain-size analyzer. Defloculation of the samples was done by mixing about 0.5 g of wet sediment with Calgon electrolytic solution (sodium hexametaphosphate, 20 g/L) and subsequently shaking for at least 3 h using an in-house rotator. Grain-size distribution and statistical parameters (e.g., mean, sorting) were calculated using the moment methods from the GRADISTAT software (Blott and Pye, 2001). Furthermore, the end-member modelling algorithm (EMMA) developed by Weltje (1997) and adapted by Dietze et al. (2012) was applied to the grain-size data in order to extract meaningful end-member (EMs) grain-size distributions and estimate their proportional contribution to the sediments. The cumulative explained variance (r^2) was calculated in order to assess the minimum number of EMs needed for a good estimate of our grain-size data (e.g., Weltje, 1997; Prins and Weltje, 1999; Dietze et al., 2012). A more detailed description of the EMMA method applied can be found in Dietze et al. (2012). Overall, grain-size distribution and end-member modelling analysis were used to investigate the sedimentary transfer regime because sediment grain-size distribution (primarily driven by sedimentary processes) reflects transport conditions (e.g., Montero-Serrano et al., 2009, 2010; Simon et al., 2012; Dietze et al. 2012; Stuut et al., 2014) (**Figure 3**).

3.3.4. *Bulk sediment mineralogy*

The random powder samples were side-loaded into the holders and analysed by X-ray diffraction (XRD) using a PANalytical X'Pert Powder diffractometer. This instrument is fitted with a copper tube (Cu K-alpha = 1.54178Å) operating at 45 kV and 40 mA and a post-diffraction graphite monochromator. Samples were scanned from 5° to 65° two-theta in steps of 0.02° two-theta and a counting time of 2 seconds per step. For the semi-quantification of the major mineralogical components, the bulk sediment XRD scans obtained were processed in the software package X'Pert High-Score Plus (PANalytical) using the Rietveld full-pattern fitting method (e.g., Young, 1993; Grunsky et al., 2013). This method permits the semi-quantification of whole-sediment mineralogy with a precision of 5–10% for phyllosilicates and 5% for non-phyllosilicates minerals. The quality of the Rietveld fitting procedure was evaluated for two statistical agreement indices: R-profile and goodness-of-fit (GOF). R-profile quantifies the difference between the observed and calculated patterns, whereas the GOF is the ratio between the R-weighted profile (RWP; best fit of least squares between observed and calculated patterns) and R-expected theoretical (Rexp; best possible value for the residual). R-values profile between 20–30% and GOF of less than 3 are typically adequate in the Rietveld refinement of geological samples (e.g., Young, 1993). The major mineralogical components quantified by this technique are: quartz, potassium (K) feldspar (microcline + orthoclase), plagioclase feldspar (albite + anorthite), amphibole (hornblende), pyroxene (augite), magnetite, hematite, goethite, calcite, dolomite, and phyllosilicates (biotite, muscovite, illite, chlorite, and kaolinite).

3.3.5. *Elemental geochemistry*

A total of 14 elements (Al, Si, K, Mg, Ca, Ti, Mn, Fe, P, Sr, V, Cr, Zn, and Zr) were analysed by energy dispersive X-ray fluorescence (EDXRF) spectrometry using a PANalytical Epsilon 3-XL. Before EDXRF analysis, loss on ignition (LOI) was determined gravimetrically by heating the dried samples up to 950°C for two hours. Subsequently, samples were treated by borate fusion in an automated fusion furnace (CLAISSE® M4 Fluxer). Samples weighing ~0.6 g were mixed with ~6 g of lithium borate flux

(CLAISSE, pure, 49.75% $Li_2B_4O_7$, 49.75% $LiBO_2$, 0.5% LiBr). The mixtures were melted in Pt-Au crucibles (95% Pt, 5% Au), and after fusion the melts were cast to flat disks (diameter: 32 mm; height: 3 mm) in Pt–Au moulds. Acquired XRF spectra were processed with the standardless Omnian software package (PANalytical). The resulting data are expressed as weight percent (wt.% ; Al, Si, K, Mg, Ca, Ti, Mn, Fe, P) and micrograms per gram (µg/g; V, Cr, Zn, Sr, Zr). Procedural blanks always accounted for less than 1% of the lowest concentration measured in the sediment samples. Analytical accuracy and precision were found to be better than 1–5% for major elements and 5–10% for the other elements, as checked by an international standard (USGS SDC-1) and analysis of replicate samples.

3.3.6. *Magnetic remanence analyses*

The isothermal remanence magnetization (IRM), and saturated isothermal remanent magnetization (SIRM) measurements of all the sediment cores used in this study were published previously by Barletta et al. (2010). These measurements were acquired on u-channel samples at 1-cm intervals using a 2G Enterprises SRM-755 cryogenic magnetometer in order to identify and characterize the magnetic concentration, mineralogy and grain size. The IRM was imparted using a 2G Enterprises pulse magnetizer with a direct current field of 0.3 T, whereas the SIRM was imparted using a field of 0.95 T. We use the IRM/SIRM ratio measured at 0 mT (referred to as the Pseudo-S ratio, St-Onge et al., 2003) to estimate the magnetic mineralogy, with values close to 1 indicating lower coercivity minerals such as magnetite, whereas lower values indicate a contribution from higher coercivity minerals such as hematite (Stoner and St-Onge, 2007).

3.4. Statistical approach

The mineralogical and geochemical data are of a compositional nature, that is, they are vectors of non-negative values subjected to a constant-sum constraint (100%). This implies that relevant information is contained in the relative magnitudes, so statistical analysis must focus on the ratios between components (Aitchison, 1986). In this context, principal component analysis (PCA) was performed on the mineralogical and elemental geochemical datasets with the goal of finding associations with similar relative variation patterns that may be interpreted from a paleoenvironmental standpoint (e.g., von Eynatten et al., 2003; Montero-Serrano et al., 2010b; 2015; von Eynatten et al., 2016). For the PCA with mineralogical data, we selected four key minerals (quartz, K-feldspar, plagioclase, and phyllosilicates) that represented more than 97% of the overall mineral concentration in the sediment sample. For the PCA with elemental data, we used all major and minor elements analysed as well as LOI. Prior to PCA, a log-centred (clr) transform was applied to the data set (Aitchison, 1990). The clr transform is derived by dividing each variable (e.g., mineral percentage, element concentration) by the geometric mean of the composition of the individual observations and then taking the logarithm. This operation removes statistical constraints on compositional variables, such as the constant-unit sum, and allows the valid application of classical (Euclidean) statistical methods to compositional data (Aitchison, 1986; 1990). PCA was conducted with "R" software using the package "compositions" (van den Boogaart and Tolosana-Delgado, 2008) (**Figure 4**).

All the presented analytical data are available electronically in the supplementary material.

4. Results

4.1. Sediment characteristics and chronostratigraphic framework

In this study, all the sediment cores present two distinct sedimentary units. According to Barletta et al. (2010), the upper unit is composed of dark grey, bioturbated silty clays to sandy mud, whereas the lower unit is composed of lighter grey and relatively homogeneous, slightly bioturbated to massive clayey silts to silty clays (**Figure 3**). The lowermost and the uppermost units may be interpreted as glaciomarine and postglacial sediments, respectively (Josenhans and Lehman, 1999; St-Onge et al., 2003).

The mean sedimentation rates of the cores COR0602-36PC and COR0503-CL05-37PC revealed an abrupt change around 8.5 ka cal, with variations from ~300 to ~40 cm/ka (**Figure 2**). St Onge et al. (2003, 2009) detected the same kind of variations in the sedimentation rates in cores MD99-2220 and MD99-2221 collected in the lower St. Lawrence Estuary and associated this observation with a significant reduction in sediment inputs following the re-routing of the LIS meltwaters from the St. Lawrence Estuary to the Hudson Bay and Strait following the catastrophic drainage of the glacial Lake Agassiz-Ojibway at ~8.47 ka cal BP (Lajeunesse and St-Onge, 2008). However, as previously pointed out by Barletta et al. (2010), a drastic changes in sedimentation rates throughout the Holocene is not observed in the core located at the most seaward location (COR0503-CL04-36PC), possibly resulting from the scarcity of dated material prior to 8.5 ka cal BP.

4.2. Grain-size end-member

The algorithm of end-member modelling analysis EMMA revealed a four-EM model to explain more than 95% of the total variance for each core (**Figure 5**). Every core is characterized by four grain classes: end-member EM4 is associated to the very coarse silts to fine sands (30 to 234 μm), end-members EM2 and EM3 correspond to the fine to medium (6 to 18 μm) and medium to coarse (9 to 63 μm) silts, and end-member EM1 is associated to the clays (<2 μm). The relative contributions of the four end-members are plotted against age in Figure 5. The sporadic layers in coarse silts to fine sand particles (EM3 and EM4) observed in **Figure 5** most likely result from the remobilization and resuspension of coarse sediments from the shelves close to the cores triggered by wave activity, tides and storm surge. As discussed by Loring and Nota (1973), coarse-grained deposits on the shelves adjacent to the Laurentian Channel are considered to be mostly relict of glacial drift material. Based on these results and in order to elucidate down-core variations in grain-size distribution, the EM2/EM1 ratio (silts/clay) is used here to investigate sediment transfer and transport conditions in the EGSL over time.

4.3. Mineralogical and geochemical associations

Stratigraphic distributions of the bulk mineralogical and geochemical data from the three sedimentary cores studied here are available electronically in **Figure S2** (supplementary material). To gain a better understanding of the mineral and elemental associations and their relationship with sediment samples, PCA was conducted on all sediment cores (**Figure 4**). We illustrate the scores from the first two principal components of the log-centered data as these accounts for more than 90% of the total variance. According to PCA results, glaciomarine sediments in the lower St. Lawrence Estuary (COR0602-36PC) are associated mainly with phyllosilicates, K-feldspar, and Mg-Cr-Fe-Zn-Al-K-V-LOI, whereas postglacial sediments are characterized by the association of plagioclase-quartz and Si-Zr-Ti-Ca-Sr. In contrast, glaciomarine sediments in the Gulf of St. Lawrence (COR0602-36PC and COR0503-CL05-37PC) are typified mainly by the association of K-feldspar and plagioclase with Mg-Sr-Cr-K-Al-Fe and to a lesser extent with Si-Ti and Mn, whereas postglacial sediments are associated with phyllosilicates-quartz and Ca-LOI-V-Zn-Mn-Si-Ti-Zr. Note that the fine-grained glaciomarine sediments in the estuary are characterized by abundant phyllosilicates, while sediments in the gulf are dominated by K-feldspar and plagioclase (**Figure 4**). This most likely suggests that the fine-grained glaciomarine sediments in the gulf contain higher proportions of rock flour derived from glacial erosion of the crystalline rocks on the Canadian Shield (Loring and Nota, 1973).

These mineralogical and geochemical differences between the Estuary and Gulf of St. Lawrence may be related to different sediment sources and hydrodynamic sorting. Therefore, based on PCA results, we selected the phyllosilicates/(plagioclase+K-feldspar), Zn/Sr, Si/K, and Zr/Al ratios to reconstruct down-core changes in sediment provenance and transport in the EGSL over the last 10 ka cal BP. The phyllosilicates/(plagioclase+K-feldspar) ratio provides a straightforward proxy to discriminate the sediments from the South Shore (Paleozoic sedimentary rocks) from those from the North Shore

(Grenvillian metamorphic rocks). In fact, as suggested in Loring and Nota (1973) and Jaegle (2015), plagioclases and K-feldspars as well as amphibole, pyroxene, and magnetite are more abundant along the North Shore, whereas phyllosilicates, quartz, and Fe-oxides (notably, hematite and goethite) are more common along the South Shore and the Canadian Maritime Provinces (on the southwest gulf). Likewise, the fact that Zn/Sr ratios reflect sediment source is based on preferential Zn concentration in phyllosilicate minerals, whereas Sr is associated with plagioclase–K-feldspar minerals (**Figure 4**). However, because Sr may also be associated with Ca in the biogenic and detrital carbonate fraction (notably, dolomite), the presence of high concentrations of carbonates can influence this ratio. In this study, the biogenic carbonates were generally removed from all cores by weak acid treatment; however, dolomite is not always removed following this attack (**Figures 6i, 7i and 8i**). Such is the case for core COR0503-CL05-37PC, collected close to Anticosti Island, where dolomite contents (**Figure 7i**) are particularly high in some intervals (up to 12%) compared to cores COR0602-36PC and COR0602-36PC (<3%; **Figures 7i and 8i**). In these circumstances and based on the PCA results, we prefer to use the Si/K ratio rather than Zn/Sr to track changes in sediment provenance south of Anticosti Island (COR0503-CL05-37P). A high Si/K ratio reflects a greater contribution from Si-rich minerals (notably, quartz), whereas low ratios suggest the input of feldspar-rich minerals, notably K-feldspar (**Figure 4**). At the same time, changes in sediment grain size are also investigated by comparing the Zr/Al ratios. Zr is concentrated in zircon grains in the coarser fractions, whereas Al is preferentially associated to clay minerals and aluminosilicates in the fine-grained fractions (e.g., von Eynatten et al., 2012).

4.4. Laurentian Channel sediment cores

Because the last deglaciation and Holocene sediment dynamics did not evolve synchronously throughout the EGSL (e.g., Dionne et al., 1977; Barletta et al., 2010; Levac et al., 2015; Rémillard et al., in press), the mineralogical, geochemical, grain size, magnetic, and spectral reflectance results obtained for each sediment core are presented by geographic location as follows:

4.4.1. *Lower St. Lawrence Estuary: Core COR0602-36PC*

Sediments between 9 and 7.5 ka cal BP in core COR0602-36PC are mainly composed of clay (up to 80% EM1) and minor amounts of fine to medium silts (~20% EM2). This grain-size trend is reversed after 7.5 ka cal BP with the occurrence of several thin coarser layers (EM3 and EM4) (**Figure 5a**). The vertical distribution of physical, magnetic, mineralogical, and geochemical proxies reveals significant downcore variations (**Figure 6**). Indeed, the a*, Zn/Sr, and phyllosilicates/(plagioclase+K-feldspar) records display maximum values in the lowermost part of the core, which sharply decrease between 9 and 8 ka cal BP, and minimum values with few variations upwards from 8 ka cal BP to the present. Conversely, the Pseudo-S ratio, magnetic susceptibility (klf), Zr/Al ratio, and EM2/EM1 ratio show their lowest values between 9 to 8 ka cal BP, whereas higher values characterize the uppermost part of the core (7.5 ka cal BP to present). Variations in the Zr/Al ratio are well correlated with changes in the proportion of the EM2/EM1 ratio. Detrital carbonate concentrations in this sediment core are negligible (<0.5%) and no major changes are recorded over time.

4.4.2. S*outh of Anticosti Island: Core COR0503-CL04-37PC*

In core COR0503-CL05-37PC, the clay (EM1) content increases from 10 to 9 ka cal BP (up to 96% EM1) and then gradually decreases to become almost non-existent from 5 ka cal BP. The sum of all the coarse fractions (EM2 + EM3 + EM4) represents more than 80% of the particle size before 9 ka cal BP, and both the fine to medium silts (EM2) and very coarse silt to fine sand (EM4) particles have dominated over the last 6 ka cal BP (**Figure 5b**). Downcore profiles of Pseudo-S, EM2/EM1, and Zr/Al ratios show a similar stratigraphic trend, with higher values in the lowermost and uppermost parts of the core (**Figure 7**). Similarly, a* and magnetic susceptibility (klf) records show maximum values in the lowermost parts of the core (10.5–9.5 ka cal BP), whereas the lowest values are characteristically in the uppermost part. The vertical distribution of phyllosilicates/(plagioclase+K-feldspar) show maxima at the base of the core and decrease to reach its minima at 9.5 ka cal BP and then increases upwards. Similar to the mineralogical ratio, the Si/K ratio also reveals higher values between 11 and 9.5 ka cal BP, which gradually decreases until 9 ka cal BP, and then increases during the mid to late Holocene. Both phyllosilicates/(plagioclase+K-feldspar) and Si/K depict a sharp upswing centered at about 5 ka cal BP. High detrital carbonate concentrations (10–12 %) are recorded between 10.5–9.5 ka cal BP and 6.5–4 ka cal BP.

4.4.3. *Cabot Strait: Core COR0503-CL04-36PC*

In core COR0503-CL04-36PC, sediments between 10.5 and 6 ka cal BP are mainly composed of clay (up to 80% EM1), whereas fine to medium silts (EM2) and very coarse silts (EM4) dominate during the last 7 ka cal BP (**Figure 5c**). Down core profiles of Pseudo-S, phyllosilicates/(plagioclase+K-feldspar), Zn/Sr, and Zr/Al ratios mimic the stratigraphic trend of the EM2/EM1 ratio, with the lowest values between 10.5 and 7 ka cal BP and higher values during the last 7 ka cal BP (**Figure 8**). The a* records reveals minima in the lowermost (10.5–8.5 ka cal BP) and uppermost (2.5–1 ka cal BP) parts of the core, and maxima between 8.5–2.5 ka cal BP and during the last 1 ka cal BP. The magnetic susceptibility (k_{lf}) record presents maxima in the lowermost parts of the core (10.5–9 ka cal BP), which decreases abruptly at about 9 ka cal BP and peaks again until ~8 ka cal BP, then slowly decreases. Relatively higher detrital carbonate concentrations (up to 3%) are observed between 7–5 ka cal BP, 3.5–2.5 ka cal BP, and the last 1 ka cal BP.

5. Interpretation and discussion

During the last deglaciation, the earth's orbital configuration induced a strong summer insolation maximum and winter insolation minimum in the Northern Hemisphere (Berger and Loutre, 1991). This strong boreal summer insolation induced a rapid retreat of the LIS (e.g., Carlson et al., 2008, 2009;

Montero-Serrano et al., 2009, 2011). During this early stage, the rapid hinterland retreat of the LIS triggered major changes in the EGSL system, engendering alterations in proglacial drainage and relative sea-level oscillations (Dyke et al., 1987; Shaw, 2006). The long-term variations observed in our physical, mineralogical, geochemical, and magnetic records are discussed in this context in terms of changes in detrital sediment supply, provenance, and transport, and their possible relations with both the deglacial/Holocene climate variability and glacio-isostatic relative sea-level variations.

5.1. Sedimentary regime during deglaciation (11–8.5 ka) — meltwater discharges

The high sedimentation rates (~300 cm/ka) in the thick fine-grained sedimentary sequences during deglaciation (11–8.5 ka cal BP) suggest sedimentary dynamics mainly controlled by the meltwater discharge from the local retreat of the southeastern margin of the LIS on the Canadian Shield (e.g., Syvitski and Praeg, 1989; St-Onge et al., 2003; 2008). This observation is in agreement with the regional deglaciation pattern of the LIS on the Canadian Shield summarized by Shaw (2006). Indeed, around 13 ka cal BP, large marine areas of Atlantic Canada were ice free (e.g., Rémillard et al., 2016), but glaciers remained on most land areas. At 9 ka cal BP, glacier ice remained only in the Quebec and Labrador regions. Extensive emerged areas could be found on the Grand Banks and on the Scotian Shelf, and large parts of the southern Gulf of St. Lawrence had also emerged (Shaw, 2006). All these observations concurred to highlight the presence of the LIS on the North Shore in the early Holocene (Dyke and Prest, 1987; Syvitski and Praeg, 1989; Shaw et al., 2006), which may explain the large amount of meltwater discharges into the EGSL.

In the lower estuary, the phyllosilicates/(plagioclase+K-feldspar) and Zn/Sr ratios as well as the a* and Pseudo-S ratio indicate a mixed provenance of detrital particles between 9 and 8.5 ka cal BP, that is, mainly from the North Shore, but with a noticeable contribution from the South Shore. We hypothesize that this sediment mixture is likely due to the close proximity of the LIS margin to the North

Shore (e.g., Clark et al., 1978; Dyke and Peltier, 2000; Shaw et al., 2002). In fact, the greater glacio-isostatic loading by the LIS over the lower estuary compared to the Gulf induced a higher relative sea level (>100 m) during the early Holocene than at present (**Figure 9**; Clark et al., 1978; Shaw, 2006). Such conditions likely promoted an increase in coastal erosion on the South Shore and, therefore, a larger sediment supply from this area.

In the south of Anticosti Island (COR0503-CL05-37PC), mineralogical, geochemical, and magnetic variations observed between 10.5 and 9.5 ka cal BP also suggest a mixture of sediment provenances. However, the relative sea level in the Gulf is lower (~ -20 to -30 m; Shaw et al., 2002; Rémillard et al., 2016) than the lower estuary as the LIS margin is more distant (~400 km NW; Shaw, 2006; Figure 9). In agreement with Loring and Nota (1973), we hypothesize that these lowstand conditions promoted the remobilization of reddish-brown glacigenic sediments stored on the Magdalen Shelf as well as subsequent transport towards the Laurentian Channel. Surface sediments in the Magdalen Shelf are mainly composed of erosional products derived from Paleozoic sedimentary rocks of the Appalachian province, which are rich in quartz, phyllosilicates, and hematite (which imparts a reddish hue to sediments) and, to a minor extent, by glacigenic sediments derived from crystalline rocks of the Canadian Shield characterized by an abundance of feldspars, amphibole, and magnetite (Loring and Nota, 1973). The glacigenic materials from the Shield were transported to the Magdalen Shelf by southward advances of the LIS during the late Wisconsin glaciation (Loring and Nota, 1973). Very large increases in a* values (red), the Zr/Al ratio, and magnetic susceptibility (klf) observed at the base of core COR0503-CL05-37PC support the interpretation of the South Shore sedimentary origin (**Figure 7**).

Concurrently, in Cabot Strait (COR0503-CL04-36PC), the low phyllosilicates/(plagioclase+K-feldspar) and Zn/Sr ratios as well as higher Pseudo-S ratio (magnetite) and magnetic susceptibility (klf) values observed during the early Holocene suggest that the detrital sediments mainly originated from the North Shore with a minor influence from the Canadian Maritime Provinces. These results are coherent with those obtained by Stevenson et al. (2008), whose less-radiogenic εNd signatures obtained on a core taken from the upper slope of the western Grand Banks reveal an increase in the relative contribution of the North American Shield since 13 ka.

Furthermore, results obtained from the end-member modelling analysis EMMA reveal the dominance of clay and very fine detrital silt particles in the early Holocene in all sediment cores (**Figure 5**). This observation is also confirmed by the low Zr/Al ratio values, indicating high amounts of fine-grained Al-rich mineral at the base of all cores. In agreement with several sedimentological studies (e.g., Loring and Nota, 1964; Josenhans and Lehman, 1999; St-Onge et al., 2008, 2011), we hypothesize that sediment-laden meltwater plumes derived from the North Shore, together with a relatively higher sea level than today (Clark et al., 1978), induced the accumulation of fine-grained sediments in the ice-distal zones of the EGSL during deglaciation. Indeed, the weak hydrodynamic conditions prevailing in these ice-distal glaciomarine environments caused a less turbulent depositional setting and, therefore, the preferential accumulation of fine-grained sediments.

To summarize, our results suggest that, between 10 to 8.5 ka cal BP, sediment supply in the EGSL became primarily controlled by the LIS meltwaters from the North Shore and secondarily by glacio-isostatic relative sea-level variations.

5.2. Sedimentary regime during the Holocene (8.5 ka cal BP to present) — postglacial relative sea-level variations

The observed decrease in the sedimentation rate from about 300 to 40 cm/ka at ~8.5 ka cal BP (**Figure 2**) evidenced a drastic decrease in erosional processes in the EGSL as the LIS margin withdrew from its southeasternmost extent and the meltwater discharges re-routed towards Hudson Bay and Strait (St-Onge et al., 2003; 2011). Consequently, the grain size, mineralogical, geochemical, and magnetic variations observed after 8.5 ka cal BP cannot be related to changes in the extent of the LIS. Instead, variations in our detrital proxies are most likely related to relative changes in sea level in response to glacio-isostatic rebound (Clark et al., 1978; Shaw et al., 2002, 2006). According to Clark et al. (1978), the timing and magnitude of this postglacial isostatic rebound, and therefore of relative sea level, was not uniform in eastern Canada. The glacio-isostatic rebound varies spatially depending on both ice thickness and the location of a particular area relative to the ice margin (Licciardi et al., 1999; Dyke and Peltier, 2000; Dionne, 2001; Shaw et al., 2002; Rémillard et al., 2016). Accordingly, relative sea-level variations are not similar along the east–west coring transect during the last 10 ka cal BP (**Figure 9**). Indeed, one of the cores (COR0602-CL04) was sampled in the first zone (Zone 1) described by Clark et al. (1978), which recorded a sea level about 120 m higher at 10 ka cal BP than the current level, and which has been progressively decreasing to the present. The two other cores (COR0503-CL05-37PC and COR0503-CL04-36PC) were collected in the transition zone (Zones 1-2), which records a higher sea level between 10–8 ka cal BP compared to the present day then a lower relative sea level around 8 ka cal BP (around -20 m), and a progressively rising level to the present (**Figure 9**).

In this context, we compare our detrital proxies with the closest geographic curve of relative sea level in order to deduce potential relations between relative sea-level variations and sediment dynamics in the EGSL over the last 8.5 ka cal BP (**Figures 6 to 8**). Based on the regional studies of Clark et al. (1978) and Shaw et al. (2002), we selected three relative sea-level curves along the east–west coring transect: (1) the Sept-Îles curve on the North Shore was compared with core COR0602-36PC from the estuary, (2) the eastern New Brunswick curve was compared with core COR0503-CL05-37PC, and (3) the Port au Port curve on Newfoundland's west coast was compared to core COR0503-CL04-36PC. All relative sea-level curves reveal a parallel temporal evolution with grain-size, magnetic, mineralogical, and geochemical proxies (**Figures 6 to 8**). These observations suggest that glacio-isostatic relative sea-level variations have exerted a significant control on sedimentation in the EGSL over the last 8.5 ka cal BP.

In the gulf, the mineralogical and geochemical signatures of cores COR0503-CL05-37PC and COR0503-CL04-36PC indicate that detrital sediments derived primarily from the Canadian Maritime Provinces and the South Shore, as evidenced by an increase in phyllosilicates (up to 46%) and quartz (up to 28%) relative to feldspars. Based on coastal currents patterns in the EGSL (**Figure 1a**), we suggest that the Appalachian sediments observed in these cores are mainly transported via the Gaspé Current. This current has sufficient energy (21 to 42 cm/sec; Trites, 1972; Couillard, 1980) to transports Appalachian sediments from the South Shore and Canadian Maritime Provinces until the Gulf (Loring and Nota, 1973; Dufour and Ouellet, 2007). Indeed, the outward transport that integrates all currents heading toward the ocean near Honguedo Strait ranges between 0.937 Sv ± 0.233 in December and 0.460 Sv ± 0.086 in June (Galbraith et al., 2016). According to Sheng (2001), this coastal current is separated in two branches past the tip of the Gaspé Peninsula: the south branch flows over the Magdalen Shelf and along the Canadian Maritime Provinces coast, whereas the north branch flows along the western edge of the Laurentian Channel. Under this context, the south branch forms the main outflow of the Gulf on the western side of Cabot Strait and may therefore supply sediments from the Canadian Maritime Provinces to the core COR0503-CL04-36PC. Conversely, the north branch may supply to the core COR0503-CL05-37PC sediments derived mainly from the South Shore and in minor proportion from the North Shore.

However, we do not rule out that erosion of the Paleozoic sedimentary rocks cropping out along the west coast of Newfoundland might also act as a secondary sediment supply to the southern gulf. In fact, the southwestern Newfoundland coast is also characterized by calcareous brownish-red sandstones, as well as by reddish and grey limestone and dolostone (Loring and Nota, 1973) and, therefore, may also supply phyllosilicates, quartz, dolomite, and hematite to the overall sedimentation. The significant increase in a* values (red) and decrease in the Pseudo-S ratio (hematite) observed between 8.5 and 2.5 ka cal BP in core COR0503-CL04-36PC support this observation. Therefore, the detrital carbonate-rich intervals (up to 3%) observed in core COR0503-CL04-36PC (**Figure 8i**) at 7–5 ka cal BP, 3.5–2.5 ka cal BP, and the last 1 ka cal BP were most likely derived from carbonate outcrops around the southwestern Newfoundland coast. In contrast, we suggest that the carbonate-rich interval (up to 12%) observed in core COR0503-CL05-37PC (**Figure 7i**) between 6.5 and 4 ka cal BP were most likely derived from the coastal erosion of the limestone bedrock cropping out on the Anticosti Shelf as a consequence of relative sea level rise. Overall, our detrital proxies suggest that the progressive rapid relative sea-level rise recorded in the gulf since 8.5 ka cal BP promoted shifts in the positions of the shorelines and an increase in coastal erosion in the Canadian Maritime Provinces, western Newfoundland and Anticosti Shelf and, therefore, a larger sediment supply from these areas.

In the lower estuary (COR0602-36PC), the low phyllosilicates/(plagioclase+K-feldspar), Zn/Sr, and a* values as well as Pseudo-S ratio values close to 1 (magnetite) indicate a detrital sediment provenance mainly derived from the North Shore, with the South Shore contributing weakly to global sedimentation (**Figure 6**). These detrital proxies show few noticeable variations over the last 7.5 ka cal BP, indicating relatively stable sedimentation dynamics through the mid-to-late Holocene. These results are in agreement with mineralogical interpretations by Jaegle (2015) in surface marine sediments from the St. Lawrence Estuary that suggest that the North Shore is the main source of sediment supply in the St. Lawrence Estuary. Finally, the concomitant dominance of coarser particles (EM2 to EM4) in the last 7.5 ka cal BP in all sediment cores suggests that the onset of modern estuarine conditions in the EGSL occurred during the mid-Holocene.

6. Summary and conclusions

The multiproxy approach performed on three sedimentary cores recovered along an east–west transect in the Laurentian Channel (from its head to its mouth) highlights the evolution of the origin, transport, and dynamics of the detrital sediments in the EGSL since the deglaciation. Two sedimentary regimes can be distinguished based on the physical, magnetic, grain-size, mineralogical, and geochemical signature of the sediment cores (**Figure 10**):

(1) During deglaciation (10–8.5 ka cal BP), the high sedimentation rates (~300 cm/ka), together with specific mineralogical, geochemical, and magnetic signatures, suggest that sediment dynamics were mainly controlled by the sediment-laden meltwater discharges from the North Shore resulting from the rapid hinterland retreat of the southeastern margin of the LIS on the Canadian Shield. Moreover, the end-member modelling analysis EMMA and Zr/Al ratio from the three sedimentary cores reveal the dominance of clay and very fine silt detrital particles in the early Holocene, corroborating that sedimentary deposition in the Laurentian Channel took place under an ice-distal glaciomarine environment at that time.

(2) From 8.5 ka to the present, the retreat of the LIS and the subsequent postglacial movements of the continental crust triggered significant variations in relative sea level and, therefore, changes in EGSL sedimentary dynamics. Similar trends observed between the relative sea-level curves obtained by Shaw et al. (2002) and our mineralogical, geochemical, magnetic, and grain size data suggest that the RSL changes are the predominant forces acting on the EGSL sedimentary dynamics during the mid to late Holocene. In the gulf, specific detrital signatures suggest that the South Shore, Canadian Maritime Provinces and western Newfoundland coast are the primary source-area for detrital sediments, with the Canadian Shield province acting as a secondary source. Conversely, detrital supply in the lower estuary remains mainly controlled by the North Shore.

The absence of any major changes in our detrital proxies over the last 7.5 ka cal BP suggests that the onset of the modern sedimentation regime in the EGSL occurred during the mid-Holocene. Finally, our multiproxy data provide new constraints on the influence of the LIS meltwater discharges and relative sea-level variations on sediment dynamics in the EGSL since the deglaciation.

Acknowledgements

This research was funded by the FRQ-NT (*établissement de nouveaux chercheurs universitaires* to J-C Montero-Serrano) as well as by the Natural Sciences and Engineering Research Council of Canada (NSERC) through Discovery Grants to J-C Montero-Serrano and G. St-Onge. We also acknowledge the financial support of the Canadian Foundation for Innovation (CFI) and Canada Economic Development for Quebec Regions (CED) for the acquisitions of the PANalytical X-ray diffractometer (X'Pert Powder) and X-ray fluorescence (Epsilon 3-XL), respectively. We also thank Quentin Beauvais (ISMER), Joël Chassé (IML) and Marie-Pier St-Onge (ISMER) for their technical support and advice. Finally, we thank Christine Laurin for reviewing the grammar and the anonymous reviewers for their constructive comments that helped improved the manuscript.

Appendix A. Supplementary material

Supplementary data associated with this article can be found in the online version at http…

Figure S1. Comparison of magnetic susceptibility profiles of cores MD99-2221 and COR0602-36PC. Correlative magnetic features are indicated. The last age-depth point of core MD99-2221 was used in the age model of core COR0602-36PC (Figure 2).

Figure S2. Vertical distribution of the bulk mineralogical and geochemical data obtained on the sedimentary cores COR0503-CL04-36PC (a-b), COR0503-CL05-37PC (c-d) and COR0602-36PC (e-f).

References

Aitchison, J. 1986: The statistical analysis of compositional data. Monographs on statistics and applied probability. Chapman & Hall Ltd., London; reprinted in 2003 by the *Blackburn Press*, New

600 Jersey, 416 p.

601 Aitchison, J. 1990: Relative variation diagrams for describing patterns of compositional variability. 602 *Mathematical Geology*, *22*(4), 487–511.

603 Barletta, F., St-Onge, G., Stoner, J. S., Lajeunesse, P., & Locat, J. 2010: A high-resolution Holocene 604 paleomagnetic secular variation and relative paleointensity stack from eastern Canada. *Earth and* 605 *Planetary Science Letters*, *298*(1-2), 162–174.

606 Berger, A., & Loutre, M. F. 1991: Insolation values for the climate of the last 10 million years. 607 *Quaternary Science Reviews*, *10*(4), 297–317.

608 Blaauw, M. & Christen, J. A. 2011: Flexible Paleoclimate Age-Depth Models Using an Autoregressive 609 Gamma Process. *Bayesian Analysis*, *6*, 457–474.

610 Blott, S. J., & Pye, K. 2001: GRADISTAT: a grain size distribution and statistics package for the 611 analysis of unconsolidated sediments. *Earth Surface Processes and Landforms*, *26*(11), 1237– 612 1248.

613 Carlson, A. E., Clark, P. U., Haley, B. A., Klinkhammer, G. P., Simmons, K., Brook, E. J., & Meissner, 614 K. J. 2007: Geochemical proxies of North American freshwater routing during the Younger 615 Dryas cold event. *Proceedings of the National Academy of Sciences*, *104*(16), 6556–6561.

616 Carlson, A. E., LeGrande, A. N., Oppo, D. W., Came, R. E., Schmidt, G. A., Anslow, F. S., Obbink, E. 617 A. 2008: Rapid early Holocene deglaciation of the Laurentide ice sheet. *Nature Geoscience*, *1*(9), 618 620–624.

619 Carlson, A. E., Anslow, F. S., Obbink, E. A., LeGrande, A. N., Ullman, D. J., & Licciardi, J. M. 2009: 620 Surface-melt driven Laurentide Ice Sheet retreat during the early Holocene. *Geophysical* 621 *Research Letters*, *36*(24). http://doi.org/10.1029/2009GL040948

622 Clark, J. A., Farrell, W. E., & Peltier, W. R. 1978: Global changes in postglacial sea level: A numerical 623 calculation. *Quaternary Research*, *9*(3), 265–287.

COHMAP Members. 1988: Climatic changes of the last 18,000 years: observations and model simulations. *Science*, 241:1043-52.

Couillard, D. 1980 : Physico-Chimie des eaux du Golfe et de l'Estuaire Saint-Laurent. *Canadian Water Resources Journal*, *5*(4), 55–81.

D' Anglejan, B. F., & Smith, E. C. 1973: Distribution, transport, and composition of suspended matter in the St. Lawrence estuary. *Canadian Journal of Earth Sciences*, *10*(9), 1380–1396.

D'Anglejan, B. F. 1969: Preliminary observations on suspended matter in the the Gulf of St. Lawrence. *Maritime Sediments*, pp. 15–18.

De Vernal, A., St-Onge, G., & Gilbert, D. 2011. Oceanography and Quaternary geology of the St. Lawrence Estuary and the Saguenay Fjord. *IOP Conference Series: Earth and Environmental Science*, *14*, 012004. http://doi.org/10.1088/1755-1315/14/1/012004

Debret, M., Sebag, D., Desmet, M., Balsam, W., Copard, Y., Mourier, B., Winiarski, T. 2011: Spectrocolorimetric interpretation of sedimentary dynamics: The new "Q7/4 diagram." *Earth-Science Reviews*, *109*(1-2), 1–19.

Dietze, E., Hartmann, K., Diekmann, B., IJmker, J., Lehmkuhl, F., Opitz, S., Borchers, A. 2012: An end-member algorithm for deciphering modern detrital processes from lake sediments of Lake Donggi Cona, NE Tibetan Plateau, China. *Sedimentary Geology*, *243-244*, 169–180.

Dionne, J. 1993: Long-term rates of vertical accretion and modern erosion of tidal marshes of a so-called emerging shoreline, St. Lawrence estuary, Québec (p. 8). Presented at the Abstracts: *Symposium on sediment dynamics, deposition and erosion in temperate salt marshes*. International Geographic Union, Commission on Coastal Systems (Cocodrie, Louisiana, 2 au 4 avril 1993), Manuscript.

Dionne, J.-C. 1977 : La mer de Goldthwait au Québec. *Géographie physique et Quaternaire*, *31*(1-2), 61. http://doi.org/10.7202/1000055ar

Dionne, J.-C., & Pfalzgraf, F. 2001: Fluctuations holocènes du niveau marin relatif à Rivière-Ouelle, côte sud du moyen estuaire du Saint-Laurent : données complémentaires. *Géographie physique et Quaternaire*, *55*(3), 289. http://doi.org/10.7202/006856ar

Drapeau, G. 1992 : Dynamique sédimentaire des littoraux de l'estuaire du Saint-Laurent. *Géographie physique et Quaternaire*, *46*(2), 233. http://doi.org/10.7202/032907ar

Duchesne, M. J., Pinet, N., Bédard, K., St-Onge, G., Lajeunesse, P., Campbell, D. C., & Bolduc, A. 2010 : Role of the bedrock topography in the Quaternary filling of a giant estuarine basin: the Lower St. Lawrence Estuary, Eastern Canada. *Basin Research*, 22, 933-951.

Dufour, R., & Ouellet, P. 2007: Estuary and Gulf of St. Lawrence Estuary and Gulf of St. Lawrence Marine Ecosystem cosystem Overview and verview and verview and Assessment ssessment ssessment Report. http://biblio.uqar.ca/archives/30095570.pdf

Dyke, A. S., & Peltier, W. R. 2000: Forms, response times and variability of relative sea-level curves, glaciated North America. *Geomorphology*, *32*(3), 315–333.

Dyke, A. S., & Prest, V. K. 1987: Late Wisconsinan and Holocene History of the Laurentide Ice Sheet. *Géographie physique et Quaternaire*, *41*(2), 237-263. http://doi.org/10.7202/032681ar

Ebbestad, J. O. R., & Tapanila, L. 2005 : Non-predatory borings in Phanerotrema (Gastropoda), Early Silurian, Anticosti Island, Québec, Canada. *Palaeogeography, Palaeoclimatology, Palaeoecology*, *221*(3-4), 325–341. http://doi.org/10.1016/j.palaeo.2005.03.003

Galbraith, P.S., Chassé, J., Caverhill, C., Nicot, P., Gilbert, D., Pettigrew, B., Lefaivre, D., Brickman, D., Devine, L., & Lafleur, C. 2016 : Physical Oceanographic Conditions in the Gulf of St. Lawrence in 2015. *DFO Can. Sci. Advis. Sec. Res. Doc.* 2016/056. v + 90 p.

Grunsky, E.C., Drew, L.J., Woodruff, L.G., Friske, P.W.B., & Sutphin, D.M. 2013: Statistical variability of the geochemistry and mineralogy of soils in the Maritime Provinces of Canada and part of the

Northeast United States. *Geochemistry: Exploration, Environment, Analysis* 13(4), 249.

Hargrave, B. T., Bugden, G. L., Head, E. J. H., Petrie, B., Phillips, G. A., Subba Rao, D. V., & Yeats, P. A. 2007: Factors affecting seasonality of lithogenic and biogenic particle flux in a large estuarine ecosystem. *Estuarine, Coastal and Shelf Science*, *73*(3-4), 379–398.

Jaegle, M. (2015). Nature et origine des sédiments de surface de l'estuaire du Saint-Laurent. MSc thesis, Université du Québec à Rimouski, Rimouski, Canada, 83 p.

Josenhans, H., & Lehman, S. 1999: Late glacial stratigraphy and history of the Gulf of St. Lawrence, Canada. *Canadian Journal of Earth Sciences*, *36*(8), 1327–1345.

King, L. H., & MacLean, B. 1970: Origin of the outer part of the Laurentian Channel. *Canadian Journal of Earth Sciences*, *7*(6), 1470–1484.

Koutitonsky, V. G., & Bugden, G. L. 1991: The physical oceanography of the Gulf of St. Lawrence: a review with emphasis on the synoptic variability of the motion. *The Gulf of St. Lawrence: small ocean or big estuary*, *113*, 57-90.

Lajeunesse, P., & St-Onge, G. 2008: The subglacial origin of the Lake Agassiz–Ojibway final outburst flood. *Nature Geoscience*, *1*(3), 184–188.

Levac, E., Lewis, M., Stretch, V., Duchesne, K., & Neulieb, T. 2015: Evidence for meltwater drainage via the St. Lawrence River Valley in marine cores from the Laurentian Channel at the time of the Younger Dryas. *Global and Planetary Change*, *130*, 47–65.

Licciardi, J. M., Teller, J. T., & Clark, P. U. 1999: Freshwater routing by the Laurentide Ice Sheet during the last deglaciation. In U. Clark, S. Webb, & D. Keigwin (Eds.), *Geophysical Monograph Series* (Vol. 112, pp. 177–201). Washington, D. C.: American Geophysical Union. http://www.agu.org/books/gm/v112/GM112p0177/GM112p0177.shtml

Loring, D. H. & Nota, D. J. G. 1964: Recent depositional conditions in the St. Lawrence River and Gulf — A reconnaissance survey. *Marine Geology*, *2*(3), 198–235.

Loring, D. H., & Nota, D. J. G. 1973: Morphology and sediments of the Gulf of St. Lawrence. Bulletin of the Fisheries Research Board of Canada, Ottawa, v.182, 147 p. http://www.dfo-mpo.gc.ca/Library/1493.pdf

Mattheus, C. R., Rodriguez, A. B., Greene, D. L., Simms, A. R., & Anderson, J. B. 2007: Control of Upstream Variables on Incised-Valley Dimension. *Journal of Sedimentary Research*, *77*(3), 213–224.

Montero-Serrano, J. C., Bout-Roumazeilles, V., Tribovillard, N., Sionneau, T., Riboulleau, A., Bory, A., & Flower, B. 2009 : Sedimentary evidence of deglacial megafloods in the northern Gulf of Mexico (Pigmy Basin). *Quaternary Science Reviews*, *28*(27-28), 3333–3347.

Montero-Serrano, J. C., Bout-Roumazeilles, V., Sionneau, T., Tribovillard, N., Bory, A., Flower, B. P., Billy, I. 2010: Changes in precipitation regimes over North America during the Holocene as recorded by mineralogy and geochemistry of Gulf of Mexico sediments. *Global and Planetary Change*, *74*(3-4), 132–143.

Montero-Serrano, J. C., Palarea-Albaladejo, J., Martín-Fernández, J. A., Martínez-Santana, M., & Gutiérrez-Martín, J. V. 2010: Sedimentary chemofacies characterization by means of multivariate analysis. *Sedimentary Geology*, *228*(3-4), 218–228.

Montero-Serrano, J.-C., Bout-Roumazeilles, V., Carlson, A.E., Tribovillard, N., Bory, A, Meunier, G., Sionneau, T., Flower, B.P., Martinez, P., Billy, I., & Riboulleau, R. 2011. Contrasting rainfall patterns over North America during the Holocene and Last Interglacial as recorded by sediments of the northern Gulf of Mexico. *Geophysical Research Letters*, 38, L14709, doi:10.1029/2011GL048194.

Montero-Serrano, J.-C., Föllmi, K. B., Adatte, T., Spangenberg, J. E., Tribovillard, N., Fantasia, A., & Suan, G. 2015 : Continental weathering and redox conditions during the early Toarcian Oceanic Anoxic Event in the northwestern Tethys: Insight from the Posidonia Shale section in the Swiss

Jura Mountains. *Palaeogeography, Palaeoclimatology, Palaeoecology*, *429*, 83–99. http://doi.org/10.1016/j.palaeo.2015.03.043

Neumeier, U. 2011: Boulder transport by ice on a St. Lawrence salt-marsh, pattern of pluriannual movements. In *Proceedings of the coastal sediments* (pp. 2533–2545). World Scientific.

Pinet, N., Brake, V., Campbell, C., & Duchesne, M. 2011: Seafloor and Shallow Subsurface of the St. Lawrence River Estuary. *Geoscience Canada*, *38*(1), 31-40.

Piper, D.J.W., Mudie, P.J., Fader, G.B., Josenhans, H.W., MacLean, B., Vilks, G. 1990: Quaternary geology, chapter 10. In *Geology of the Continental Margin of Eastern Canada. Geological Survey of Canada* (pp. 475–607).

Prins, M., & Weltje, G. J. 1999: End-member modeling of siliciclastic grain-size distributions: The late Quaternary record of eolian and fluvial sediment supply to the Arabian Sea and its paleoclimatic significance. *SEPM Special Publication*, *62*.

Rémillard, A. M., St-Onge, G., Bernatchez, P., Hétu, B., Buylaert, J.-P., Murray, A. S., & Vigneault, B. 2016: Chronology and stratigraphy of the Magdalen Islands archipelago from the last glaciation to the early Holocene: new insights into the glacial and sea-level history of eastern Canada. *Boreas*. 10.1111/bor.12179. ISSN 0300-9483.

Saucier, F. J. 2003: Modeling the formation and circulation processes of water masses and sea ice in the Gulf of St. Lawrence, Canada. *Journal of Geophysical Research*, *108*(C8). http://doi.org/10.1029/2000JC000686

Scully, M. E., & Friedrichs, C. T. 2007: Sediment pumping by tidal asymmetry in a partially mixed estuary. *Journal of Geophysical Research*, *112*(C7). http://doi.org/10.1029/2006JC003784

Shaw, J., Gareau, P., & Courtney, R. C. 2002: Palaeogeography of Atlantic Canada 13–0kyr. *Quaternary Science Reviews*, *21*(16), 1861–1878.

Shaw, J., Piper, D. J. W., Fader, G. B. J., King, E. L., Todd, B. J., Bell, T., Liverman, D. G. E. 2006. A conceptual model of the deglaciation of Atlantic Canada. *Quaternary Science Reviews*, *25*(17-18), 2059–2081.

Sheng, J. 2001: Dynamics of a buoyancy-driven coastal jet: The Gaspe Current. *Journal of Physical Oceanography*, *31*(11), 3146–3162.

Simon, Q., St-Onge, G., & Hillaire-Marcel, C. 2012: Late Quaternary chronostratigraphic framework of deep Baffin Bay glaciomarine sediments from high-resolution paleomagnetic data: Baffin bay Late Quaternary stratigraphy. *Geochemistry, Geophysics, Geosystems*, *13*(11), http://doi.org/10.1029/2012GC004272

Stevenson, R. K., Hollings, P., Meng, X. W., & Hillaire-Marcel, C. 2008: Impact of melting of the Laurentide Ice Sheet on sediments from the upper continental slope off southeastern Canada: evidence from Sm–Nd isotopes. *Canadian Journal of Earth Sciences*, *45*(11), 1243–1252.

St-Onge, G., Stoner, J. S., & Hillaire-Marcel, C. 2003: Holocene paleomagnetic records from the St. Lawrence Estuary, eastern Canada: centennial- to millennial-scale geomagnetic modulation of cosmogenic isotopes. *Earth and Planetary Science Letters*, *209*(1-2), 113–130.

St-Onge, G., Mulder, T., Francus, P., & Long, B. 2007: Chapter Two Continuous Physical Properties of Cored Marine Sediments. In *Developments in Marine Geology* (Vol. 1, pp. 63–98). Elsevier. http://linkinghub.elsevier.com/retrieve/pii/S157254800701007X

St-Onge, G., Lajeunesse, P. 2007: Flood-induced turbibites from northern Hudson Bay and western Hudson Strait : a two-pulse record of Lake Agassiz final outburst flood ? In : V. Lykousis, D. Sakellariou et J. Locat (Eds.), *Submarine Mass Movements and Their Consequences*. Springer, 129-137.

St-Onge, G., Lajeunesse, P., Duchesne, M. J., & Gagné, H. 2008: Identification and dating of a key Late Pleistocene stratigraphic unit in the St. Lawrence Estuary and Gulf (Eastern Canada). *Quaternary Science Reviews*, *27*(25-26), 2390–2400.

St-Onge, G., & Long, B. F. 2009: CAT-scan analysis of sedimentary sequences: An ultrahigh-resolution paleoclimatic tool. *Engineering Geology*, *103*(3-4), 127–133.

St-Onge, G., Duchesne, M. J., & Lajeunesse, P. 2011: Marine geology of the St. Lawrence Estuary. *IOP Conference Series: Earth and Environmental Science*, *14*, 012003. http://doi.org/10.1088/1755-1315/14/1/012003

Stoner, J. S., & St-Onge, G. 2007: Chapter Three Magnetic Stratigraphy in Paleoceanography: Reversals, Excursions, Paleointensity, and Secular Variation. In *Developments in Marine Geology* (Vol. 1, pp. 99–138). Elsevier. Retrieved from http://linkinghub.elsevier.com/retrieve/pii/S1572548007010081

Stuut, J.-B. W., Temmesfeld, F., & De Deckker, P. 2014: A 550 ka record of aeolian activity near North West Cape, Australia: inferences from grain-size distributions and bulk chemistry of SE Indian Ocean deep-sea sediments. *Quaternary Science Reviews*, *83*, 83–94.

Syvitski, J. P. M., & Praeg, D. B. 1989: Quaternary Sedimentation in the St. Lawrence Estuary and Adjoining Areas, Eastern Canada: An Overview Based on High-Resolution Seismo-Stratigraphy. *Géographie physique et Quaternaire*, *43*(3), 291. http://doi.org/10.7202/032784ar

Tang, C. L., and Bennett A.S. 1981: Physical oceanographic observations in the northwestern Gulf of St. Lawrence. Data series BI-D-810–6, Bedford Inst. Oceanogr., Dartmouth, Canada, 127.

Trites, R. W. 1972: The Gulf of St. Lawrence from a pollution point of view, in Marine Pollution and Sea Life, M. Ruivo, ed., FAO, *FishingNews Books*, London, 59-62.

Van den Boogaart, K. G., & Tolosana-Delgado, R. 2008: “Compositions”: a unified R package to analyze compositional data. *Computers & Geosciences*, *34*(4), 320–338.

Von Eynatten, H., Barceló-Vidal, C., & Pawlowsky-Glahn, V. 2003: Composition and discrimination of sandstones: a statistical evaluation of different analytical methods. *Journal of Sedimentary Research*, *73*(1), 47–57.

Von Eynatten, H., Tolosana-Delgado, R., & Karius, V. 2012: Sediment generation in modern glacial settings: Grain-size and source-rock control on sediment composition. *Sedimentary Geology*, *280*, 80–92.

Von Eynatten, H., Tolosana-Delgado, R., Karius, V., Bachmann, K., & Caracciolo, L. 2016: Sediment generation in humid Mediterranean setting: Grain-size and source-rock control on sediment geochemistry and mineralogy (Sila Massif, Calabria). *Sedimentary Geology*, *336*, 68–80.

Webb III, T., Anderson, K. H., Bartlein, P. J., & Webb, R. S. 1998: Late Quaternary climate change in Eastern North America: A comparison of pollen-derived estimates with climate model results. *Quaternary Science Reviews*, *17*(6), 587–606.

Weltje, G. J. 1997: End-member modeling of compositional data: numerical-statistical algorithms for solving the explicit mixing problem. *Mathematical Geology*, *29*(4), 503–549.

Young, R.A., 1993: The Rietveld Method. International Union of Crystallography Monographs on Crystallography 5. [Chester, England]: Oxford; New York: International Union of Crystallograhy; Oxford University Press, 308 p.

Table caption

Table 1. Coordinates and lengths of the three sedimentary piston cores studied herein.

Figure captions

Figure 1. (a) Simplified oceanic circulation models from the Estuary and Gulf of St.Lawrence (modified from Galbraith et al., 2016) between October to December (black vectors) and April to June (blue vectors). (b) Simplified geological map of the land adjacent to the Estuary and Gulf of St. Lawrence (modified from Loring et al., 1973) show the location of the three sedimentary piston cores studied herein.

Figure 2. Age models for cores COR0602-36PC, COR0503-CL05-37PC, and COR0503-CL04-36PC. Modified from Barletta et al. (2010).

Figure 3. Mean grain size versus depth for cores COR0602-36PC, COR0503-CL05-37PC and COR0503-CL04-36PC. The grey and orange areas represent glaciomarine and postglacial sediments, respectively. The sediment texture is indicated to the right of each diagram. St-c = Silty clays; C-st = Clayey silts; St = Silts; S-md = Sandy muds. From Barletta et al. (2010).

Figure 4. Biplots of the PC-1 versus PC-2 obtained from the log-centred transformation of the bulk mineralogical and geochemical data for cores COR0602-36PC (a), COR0503-CL05-37PC (b) and COR0503-CL04-36PC (c).

Figure 5. End-member modelling analyses (EMMA) performed on the grain-size distribution of the detrital fraction of cores COR0602-36PC (a), COR0503-CL05-37PC (b) and COR0503-CL04-36PC (c). The grain-size distribution of the four first end-members accounts for more than 95% of the total variance. Four representative unmixed grain-size distributions as well as end-member scores (%) derived from EMMA are shown.

Figure 6. Multiproxy analysis for core COR0602-36PC. (a) relative sea level variations at Sept-Iles (Shaw et al., 2002); (b) geochemical ratio Zn/Sr; (c) mineralogical proxies phyllosilicates/(plagioclase+K-feldspar); (d) grain-size parameters EM2/EM1; (e) geochemical ratio Zr/Al; (f) Pseudo S ratio magnetic parameter; (g) magnetic susceptibility (k_{lf}); (h) a* indicates sediment colour variations from green to red; (i) Dolomite content variations.

Figure 7. Multiproxy analysis for core COR0503-CL05-37PC. (a) relative sea level at the eastern New Brunswick (Shaw et al., 2002); (b) geochemical ratio Si/K; (c) mineralogical proxies phyllosilicates/(plagioclase+K-feldspar); (d) grain-size parameters EM2/EM1; (e) geochemical ratio Zr/Al; (f) Pseudo S ratio magnetic parameter; (g) magnetic susceptibility (k_{lf}); (h) a* indicates sediment colour variations from green to red; (i) Dolomite content variations.

Figure 8. Multiproxy analysis for sedimentary core COR0503-CL04-36PC. (a) relative sea level at Port au Port (Shaw et al., 2002); (b) geochemical ratio Zn/Sr; (c) mineralogical proxies phyllosilicates/(plagioclase+K-feldspar); (d) grain-size parameters EM2/EM1; (e) geochemical ratio Zr/Al; (f) Pseudo S ratio magnetic parameter; (g) magnetic susceptibility (k_{lf}); (h) a* indicates sediment colour variations from green to red; (i) Dolomite content variations.

Figure 9. Evolution of the relative sea level over the last 10,000 years (Shaw et al., 2002) represented on the A-B transect (Pointe-des-Monts – Cabot Strait). The different zones specified by Clark et al. (1978) have been represented: the First Zone had a relative sea level 120 m higher at 10 ka cal BP and progressively decreases until today; the Transition Zone (Zones 1–2) had a higher sea level followed by a lower relative sea level around 8 ka cal BP, and a gradual re-increase in sea level after that. The positions of the three sedimentary cores studied here are also shown.

Figure 10. Evolution of sedimentary dynamics between 10-8.5 ka cal BP and since the last 8.5 ka cal BP. During the early Holocene (a), the sedimentary dynamics is mainly controlled by the meltwater discharges due to the rapid retreat of the southeastern margin of the LIS on the North Shore. The sedimentary contribution of the Appalachians is induced by a high relative sea level in the estuary and by a low relative sea level in the gulf, causing a strong erosion of the Magdalen Shelf (modified from Shaw

et al., 2002). From 8.5 ka cal BP to the present (b), variations in relative sea level represent the predominant forces acting on the EGSL sedimentary dynamics. A sharp discrimination of sedimentary sources appears, with the North Shore becoming the main sediment supply in the estuary whereas the South Shore appears as the main sedimentary sources in the gulf.

FIGURE 1
(Full Page width)

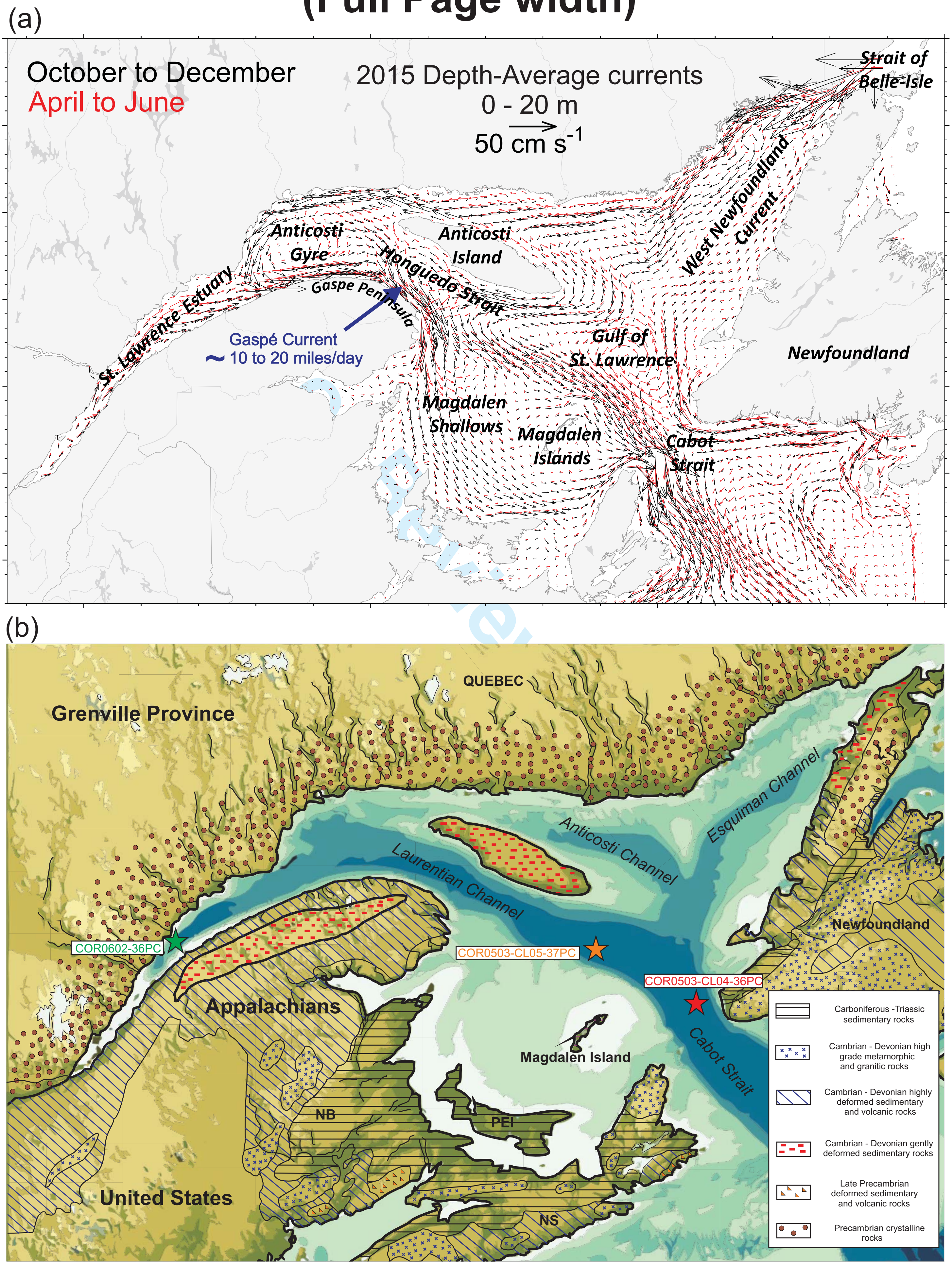

Figure 2
(One and a half page width)

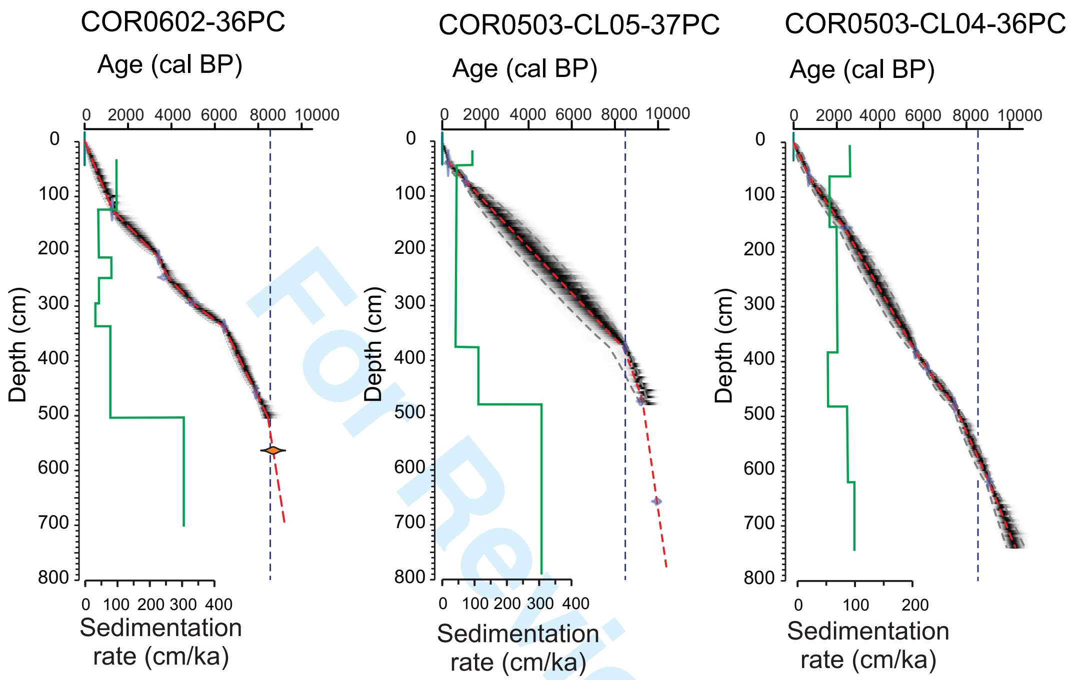

FIGURE 3
(Full page width)

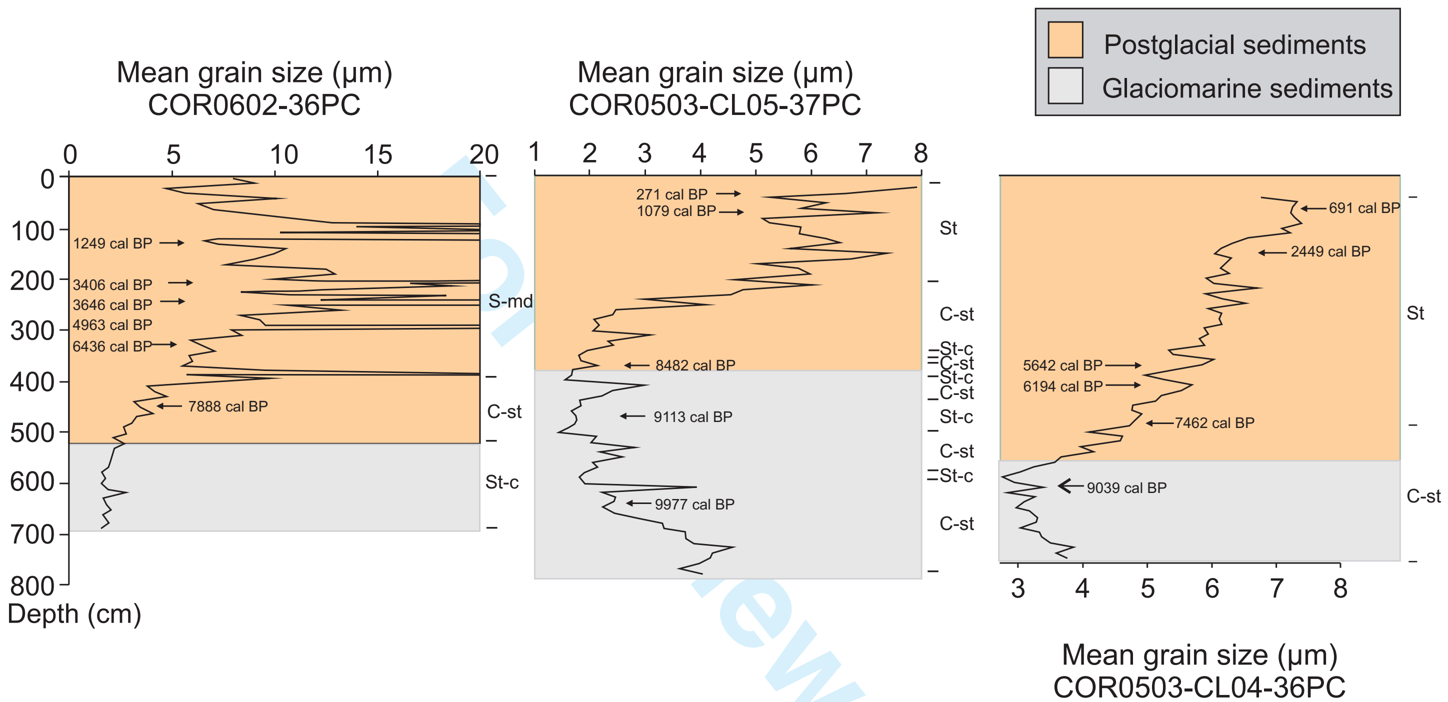

FIGURE 4
(One and a half page width)

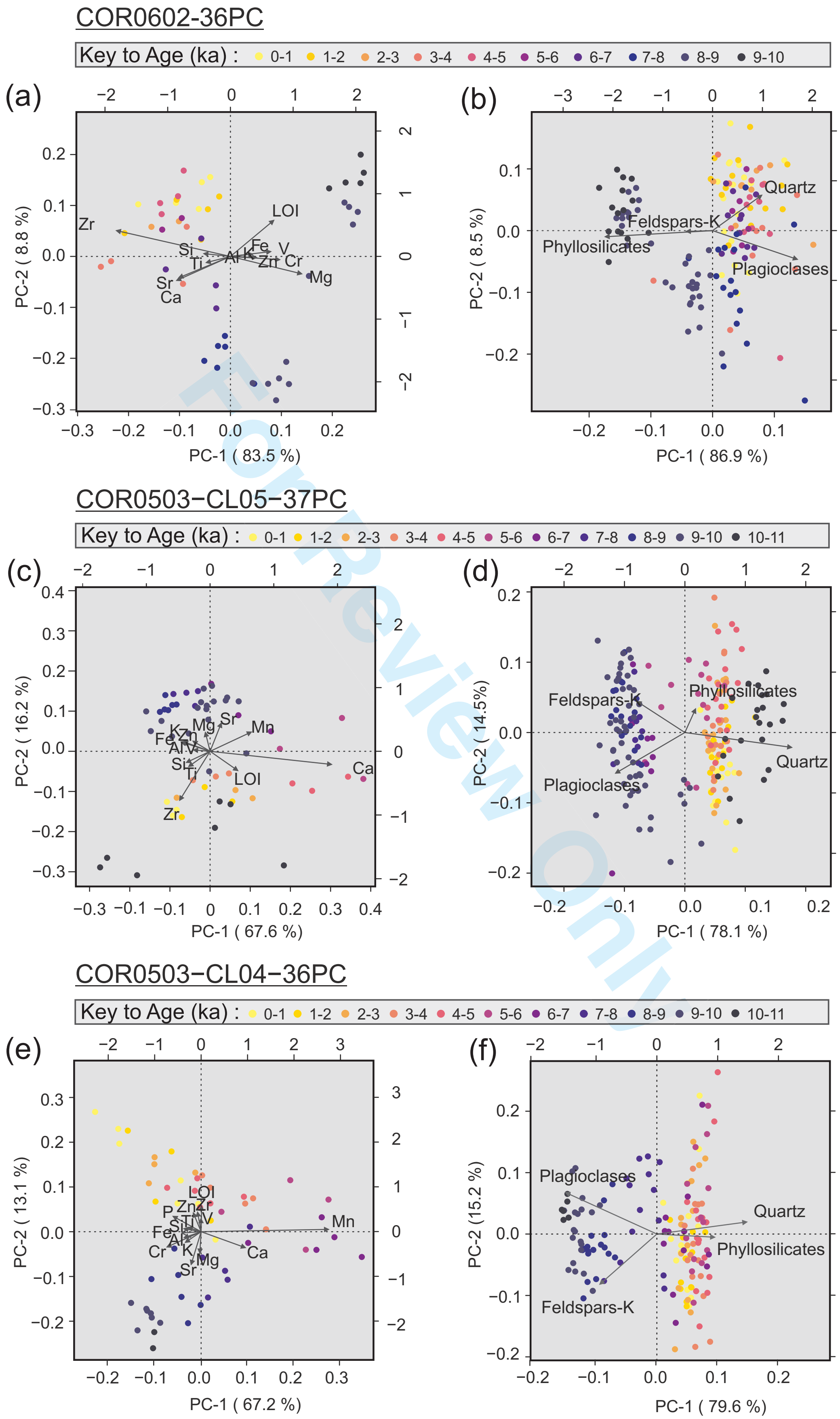

Figure 5
(Full page width)

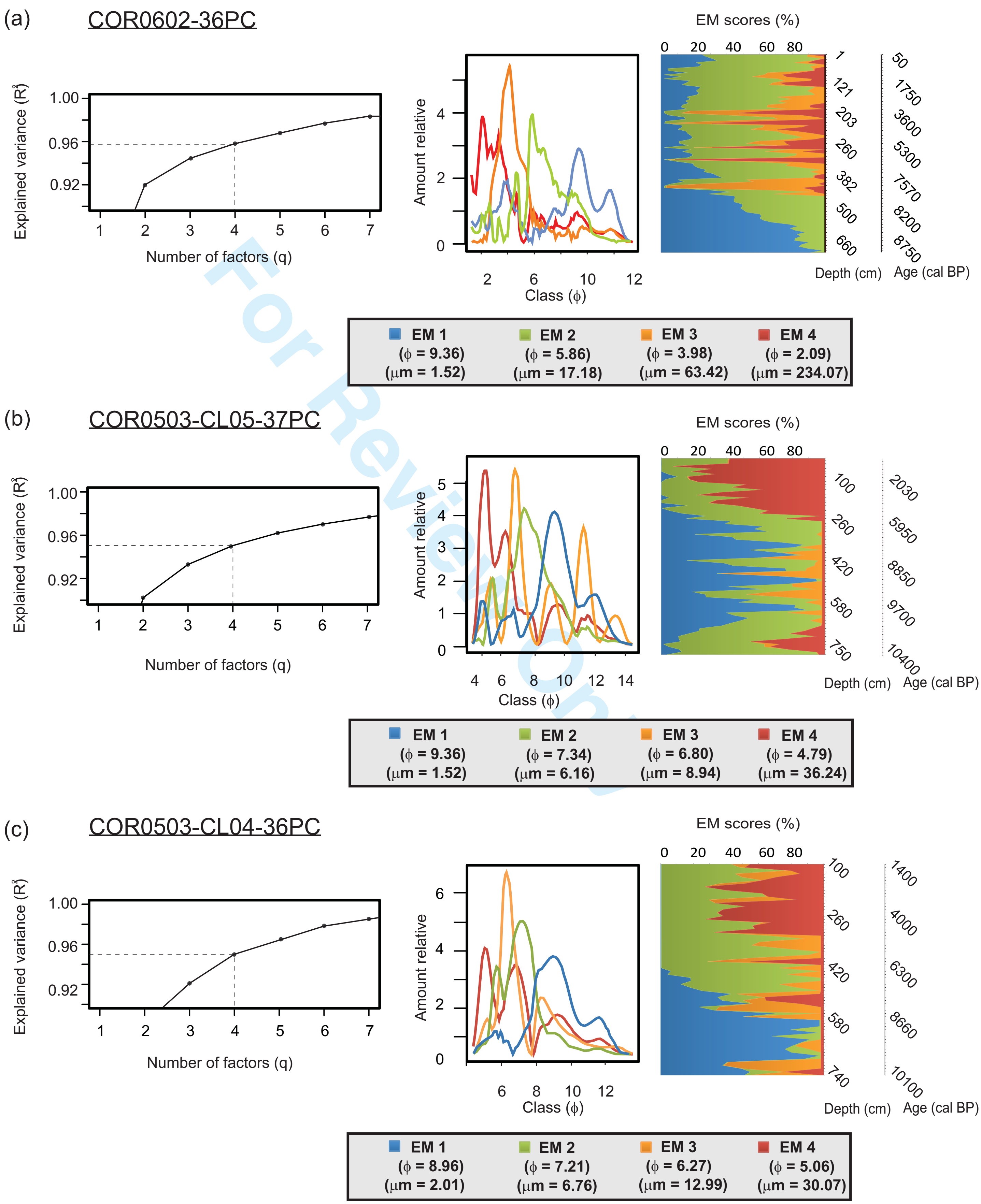

Figure 6
(One and a half page width)

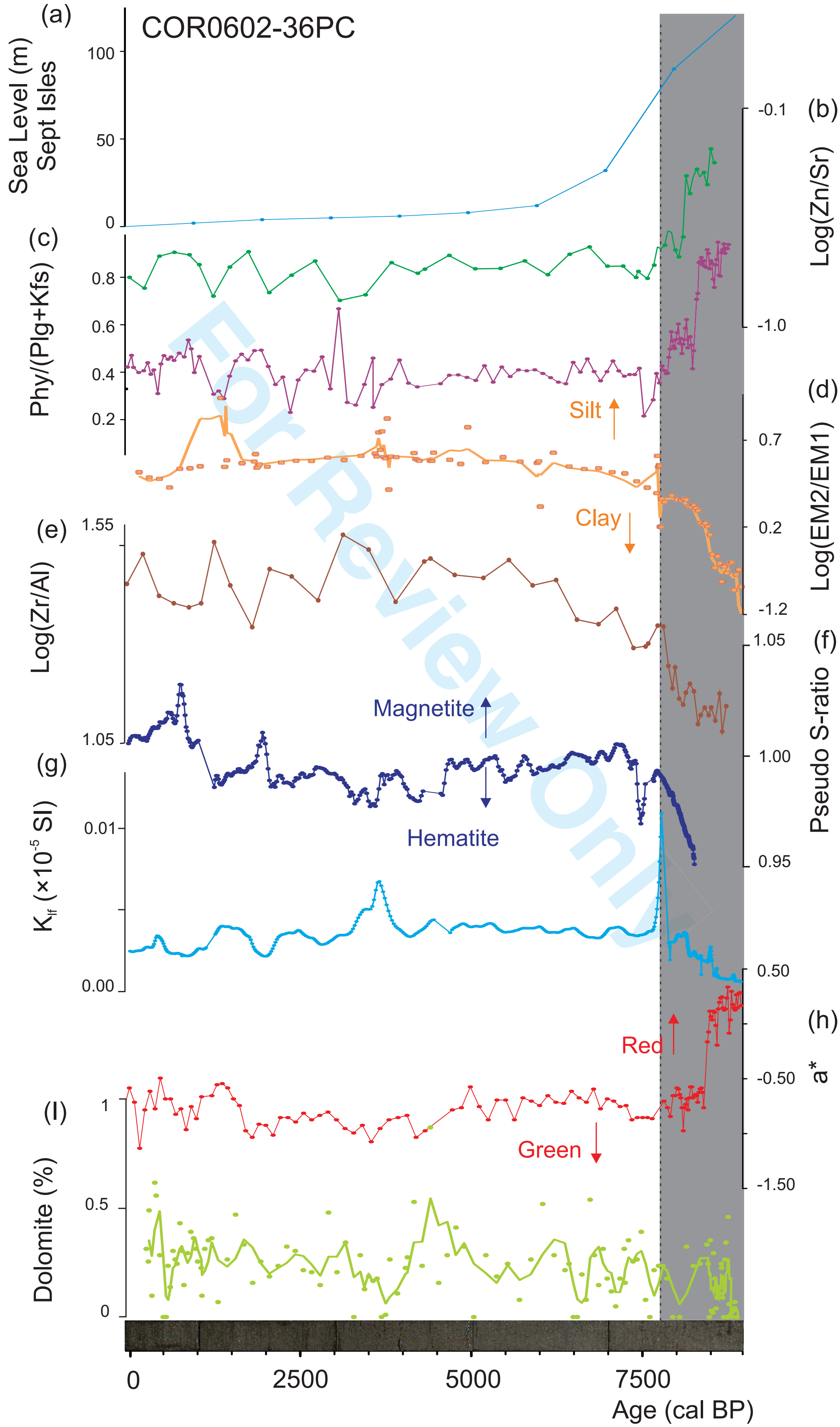

Figure 7
(One and a half page width)

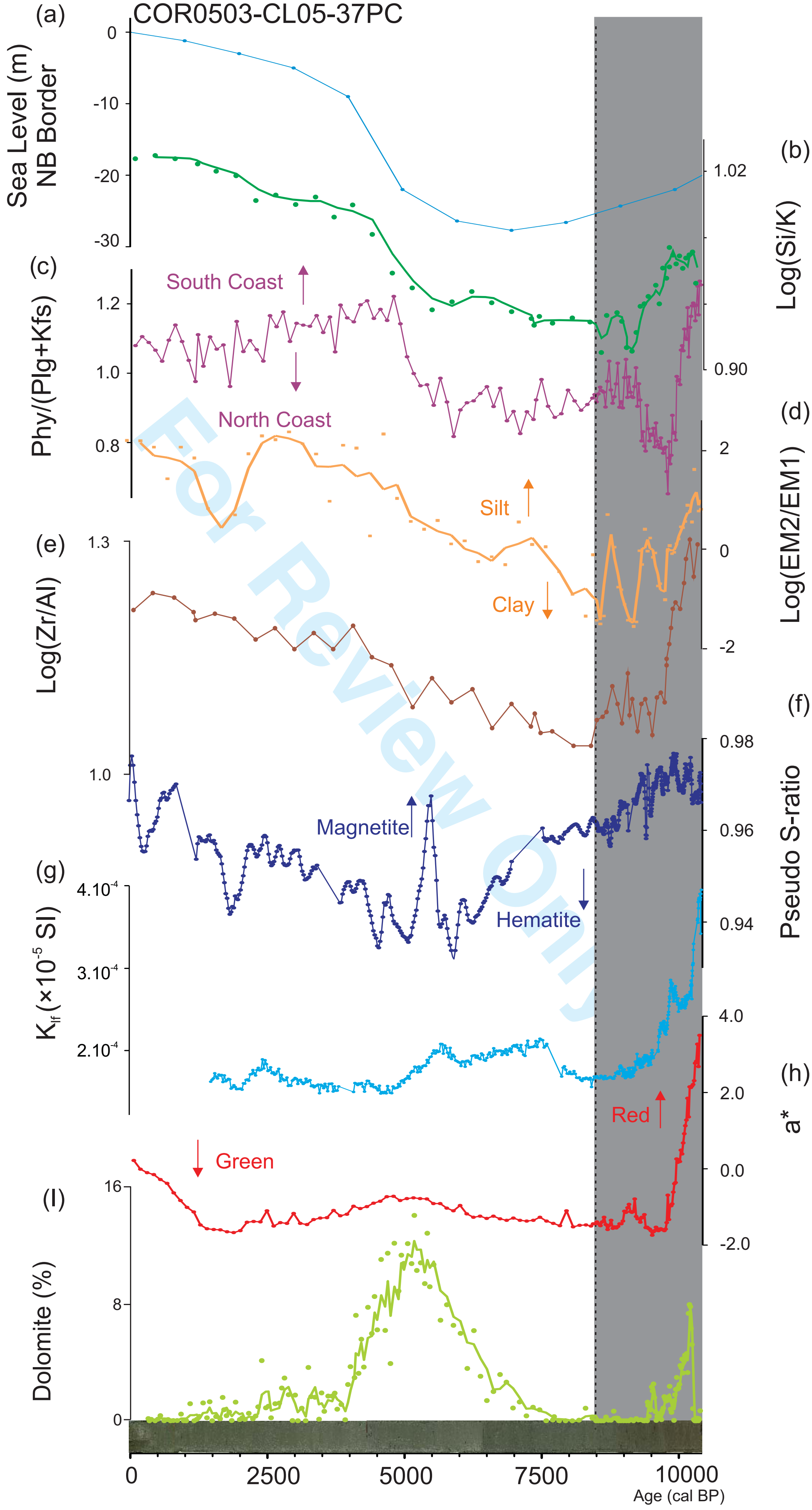

Figure 8
(One and a half page width)

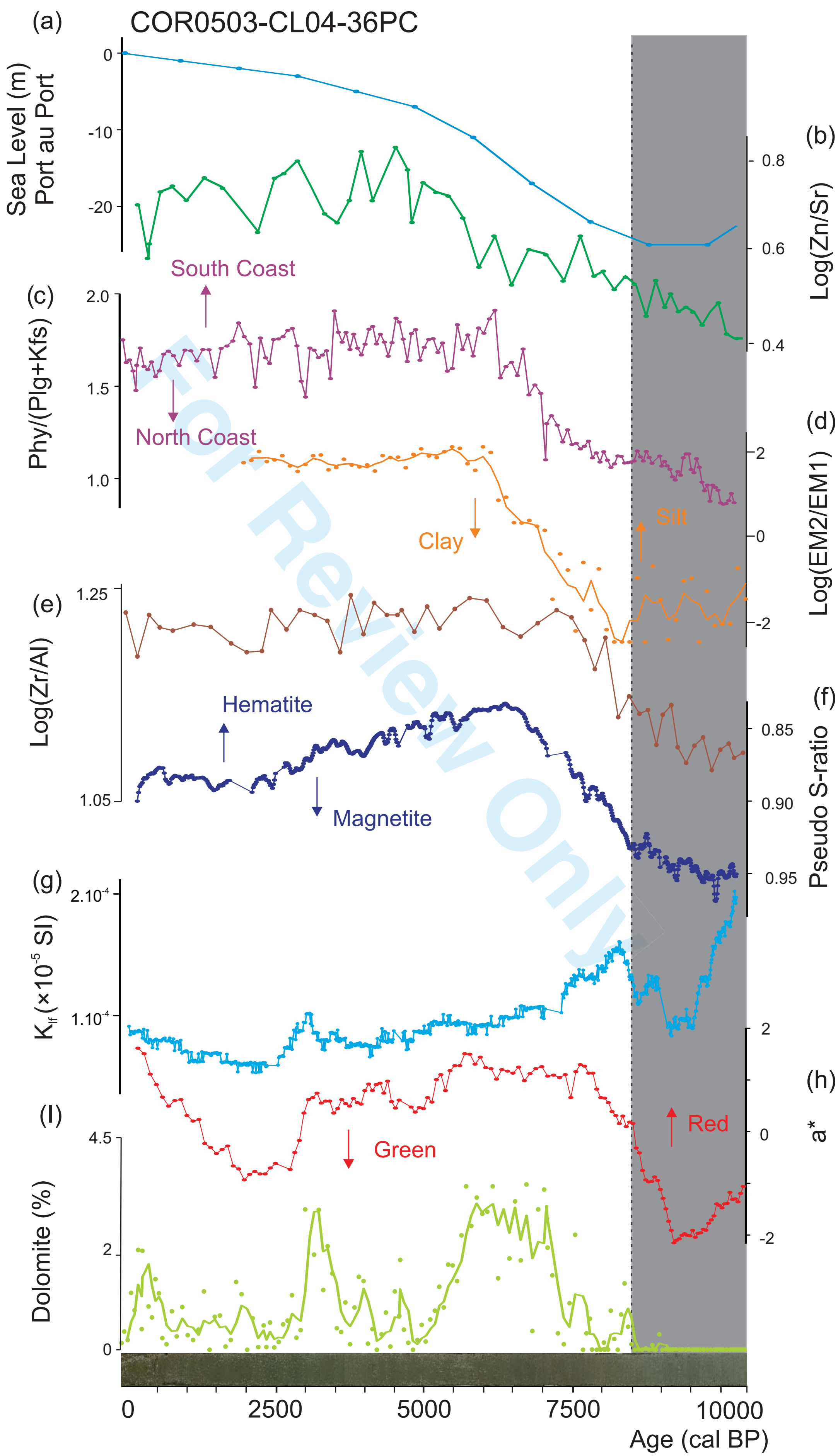

FIGURE 9
(One and a half page width)

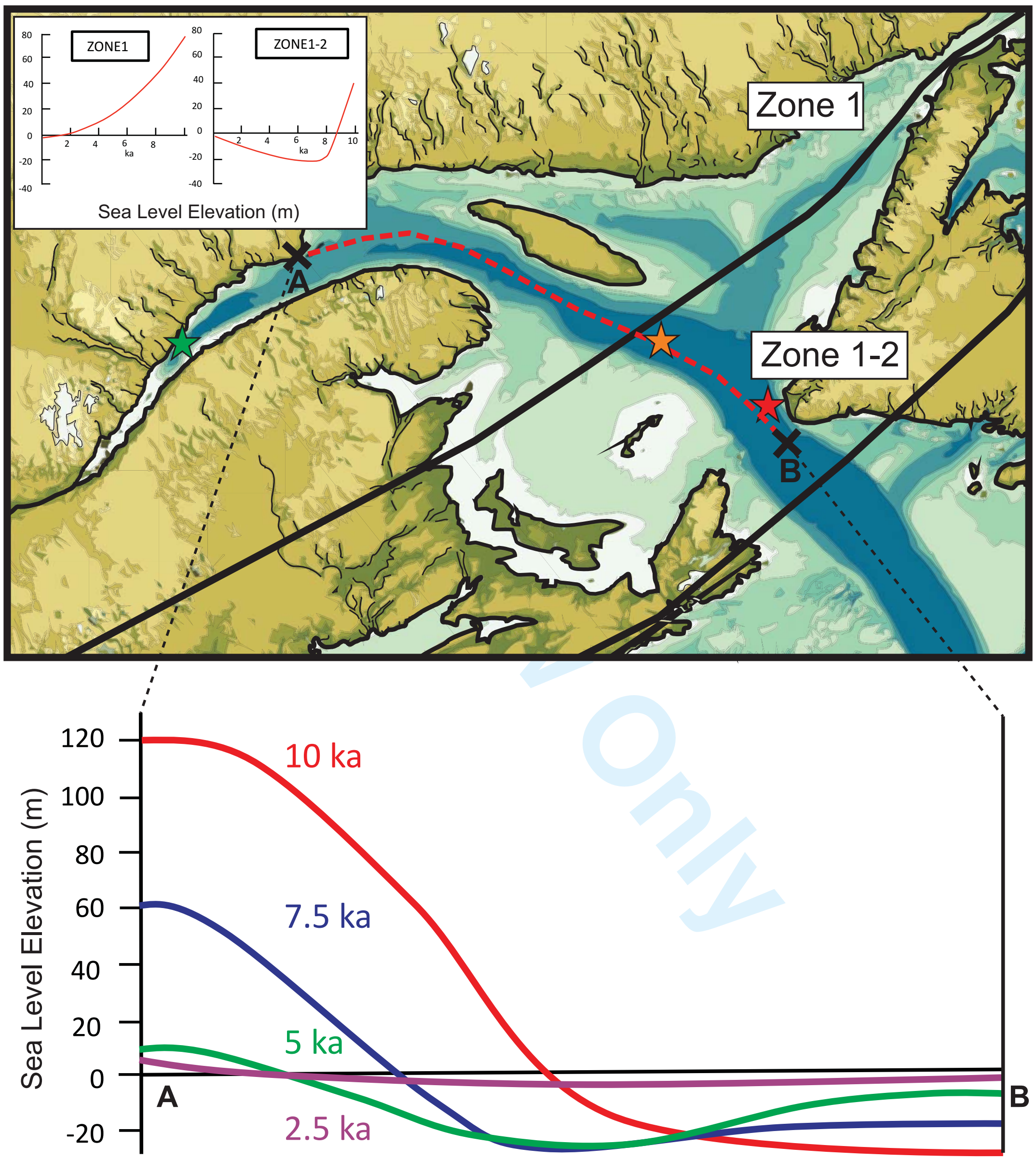

figure 10

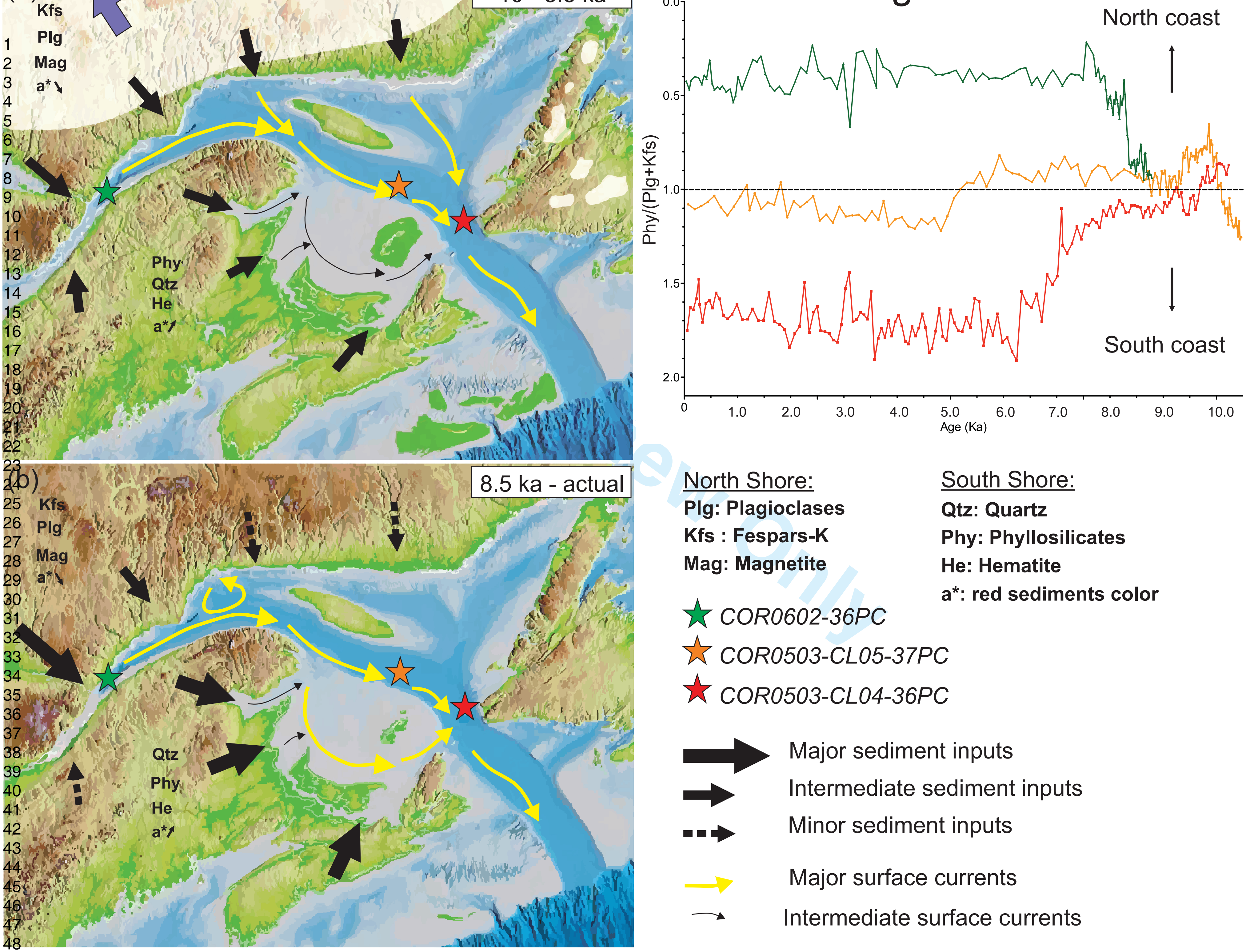
(a)
10 - 8.5 ka
Kfs
Plg
Mag
a*
Phy
Qtz
He
a*
(b)
8.5 ka - actual
Kfs
Plg
Mag
a*
Qtz
Phy
He
a*
Phy/(Plg+Kfs)
0.0
0.5
1.0
1.5
2.0
0
1.0
2.0
3.0
4.0
5.0
6.0
7.0
8.0
9.0
10.0
Age (Ka)
North coast
South coast
North Shore:
Plg: Plagioclases
Kfs : Fespars-K
Mag: Magnetite
South Shore:
Qtz: Quartz
Phy: Phyllosilicates
He: Hematite
a*: red sediments color
COR0602-36PC
COR0503-CL05-37PC
COR0503-CL04-36PC
Major sediment inputs
Intermediate sediment inputs
Minor sediment inputs
Major surface currents
Intermediate surface currents

Supplementary material
Figure S1

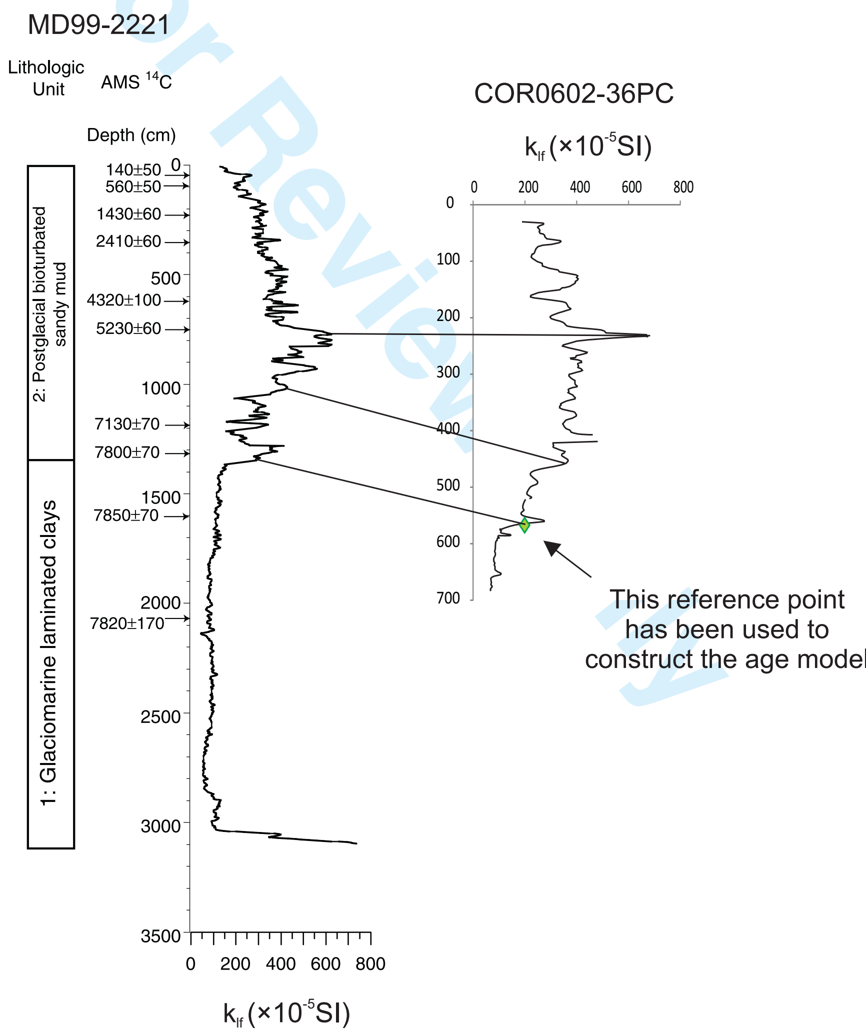

Figure S2

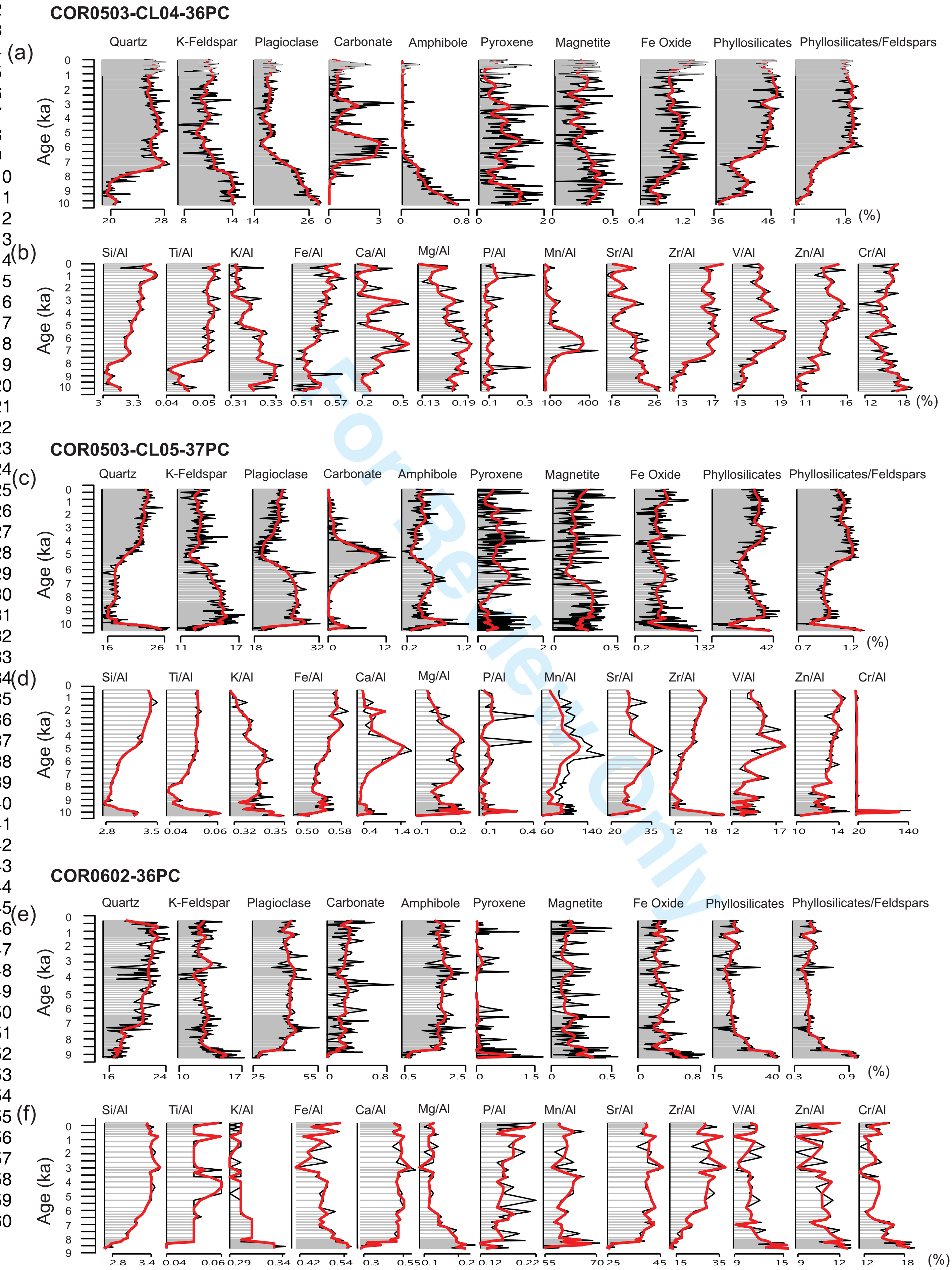
COR0503-CL04-36PC
(a)
Quartz
K-Feldspar
Plagioclase
Carbonate
Amphibole
Pyroxene
Magnetite
Fe Oxide
Phyllosilicates
Phyllosilicates/Feldspars
Age (ka)
(%)
(b)
Si/Al
Ti/Al
K/Al
Fe/Al
Ca/Al
Mg/Al
P/Al
Mn/Al
Sr/Al
Zr/Al
V/Al
Zn/Al
Cr/Al
Age (ka)
(%)
COR0503-CL05-37PC
(c)
Quartz
K-Feldspar
Plagioclase
Carbonate
Amphibole
Pyroxene
Magnetite
Fe Oxide
Phyllosilicates
Phyllosilicates/Feldspars
Age (ka)
(%)
(d)
Si/Al
Ti/Al
K/Al
Fe/Al
Ca/Al
Mg/Al
P/Al
Mn/Al
Sr/Al
Zr/Al
V/Al
Zn/Al
Cr/Al
Age (ka)
COR0602-36PC
(e)
Quartz
K-Feldspar
Plagioclase
Carbonate
Amphibole
Pyroxene
Magnetite
Fe Oxide
Phyllosilicates
Phyllosilicates/Feldspars
Age (ka)
(%)
(f)
Si/Al
Ti/Al
K/Al
Fe/Al
Ca/Al
Mg/Al
P/Al
Mn/Al
Sr/Al
Zr/Al
V/Al
Zn/Al
Cr/Al
Age (ka)
(%)

Table 1

One and a half page width

Cores	Latitude (°N)	Longitude (°W)	Water depth (m)	Length (m)
COR0602-36	48°24.031’	69°14.328’	315	6.97
COR0503-CL04-36	47°40.2860’	59°59.9850’	544	7.71
COR0503-CL05-37	48°20.0110’	61°29.9950’	408	7.90